Seismic Response and Potential Failure Mechanism of Wrap-Faced Geosynthetic Reinforced Soil (GRS) Walls with Marginal Backfill

Mihretab Madamo[1,2] and Arindam Dey[3]

Mihretab Madamo

[1]Research Scholar, Department of Civil Engineering, Indian Institute of Technology Guwahati, Assam, India.

[2]Lecturer, Civil Engineering Department, Wachemo University, Hossana, 667, Ethiopia

ORCID No.: 0009-0001-0522-7269 Email: mabmadamo@gmail.com

Arindam Dey*

[3]Associate Professor, Department of Civil Engineering and Center for Disaster Management and Research, Indian Institute of Technology Guwahati, Assam, India. ORCID No.: 0000-0001-7007-2729 Contact No.: +918011002709 Email: arindam.dey@iitg.ac.in

* Corresponding author

Compliance with Ethical Standards

Conflict of Interest: The authors declare that they have no known competing financial interests or personal relationships that could have appeared to influence the work reported in this paper.

Ethical Approval: This article does not contain any studies with human participants or animals performed by any of the authors.

Author Contributions: MM: Conceptualization, Methodology, Formal analysis, Data curation and interpretation, Software, Validation, Visualization, Writing-original draft, Reviewing and editing; AD: Conceptualization, Methodology, Interpretation, Supervision, Writing-reviewing and editing

Data Availability Statement: The data pertaining to and reported in this study is available from the corresponding author upon reasonable request.

Seismic Response and Potential Failure Mechanism of Wrap-Faced Geosynthetic Reinforced Soil (GRS) Walls with Marginal Backfill

Abstract

Geosynthetic-reinforced soil (GRS) walls have become a widely adopted alternative to conventional rigid retaining structures due to their cost-effectiveness and ease of construction in difficult terrains, and higher flexibility. Among different fascia types popularly used, GRS walls with wraparound fascia offer improved flexibility while enhancing local stability. With the increasing unavailability of desired granular backfill, especially in the mountainous and hilly terrains of north-eastern India, utilization of locally available marginal soils as reinforced fill material is increasing to meet the demand. However, the response of such wrap-faced GRS wall, especially under seismic scenarios as frequently encountered in earthquake prone zones, remain quite unexplored. This study investigates and reports the response of wrap-faced GRS walls with marginal backfill under static, pseudo-static, and dynamic conditions. In this context, finite element analyses of GRS walls with wraparound fascia are carried out by incorporating variations in reinforcement stiffness and cohesion of the marginal backfill cohesion. Under gravity loading, a triangular wedge develops in the retained fill, while the reinforced fill exhibit a potential bilinear failure mechanism, and that the GRS wall induce deep-seated shear strain concentrations within the retained fill, thereby adding up to the stability of the system. Owing to the stress reversals and redistributions by the flexible reinforcements and fascia, the strength reduction factor (SRF) from the dynamic analysis are found to be more than 1.5 times higher than that of the static and pseudo-static scenarios, thereby highlighting the conservativeness of the time-independent pseudo-static designs. Compared to pseudo-static assessment, the time-history analysis of the flexible wrap-faced GRS walls are found to reduce the lateral displacements by 30%-50%. In comparison to the reinforcement stiffness, cohesion of the marginal backfill aids in the reduction of mobilized peak reinforcement load by 1.4 times to that obtained from pseudo-static analyses. Crest accelerations along the wall face is found to be amplified in the range of 2.5-4 when compared to the bottom of the wall. Potential failure surfaces are found to form approximately 0.7 m from the wall face for the bottom two-third of the wall for any combination of analyses type, backfill cohesion and reinforcement stiffness, while noticeable differences are observed for the remaining height of the wall. Although an average trend agreement might be noticed between the identified potential

failure surfaces to that of Rankine's active failure line, yet the notable differences aids in identifying the vulnerable hotspots in such wrap-faced GRS walls and calls for a more scrutinized design and rectification plans based on response assessments.

Keywords: Geosynthetic reinforced soil (GRS) walls; Wraparound fascia; Marginal backfill; Reinforcement stiffness; Pseudo-static assessment; Dynamic time-history analysis; Potential failure surface

1. INTRODUCTION

Reinforced soil (RS) wall structures have proved to be versatile alternatives to conventional retaining walls, offering advantages of cost-efficiency, rapid construction, higher load-bearing capacity, and optimized land utilization [1]. These structures comprise inclusions of natural or artificial geomaterials such as metallic reinforcements or geosynthetics, in which the latter having a preference for their durability, strength and resistance to environmental degradation, thereby making them suitable for long-term applications. Geosynthetic reinforced soil (GRS) walls employs the polymeric geosynthetics as the primary reinforcement, while the wall face can consist of various alternate constructions such as concrete panels, modular blocks, segmental blocks or even geosynthetic wraparounds. Based on the project requirement, wall height and its functionality, the fascia type of the GRS wall can be suitably selected [2]. Based on the behavior of bridge abutments, Lee and Wu [3] highlighted that GRS walls with wraparound fascia are a viable alternative to conventional bridge abutments. The 180^{o} wraparounds lead to a completely flexible fascia system, where each geosynthetic layer wrap around consecutive lifts of reinforced backfill soil with its wrap tail extending into the backfill providing anchorage to the wrap-face of the GRS wall [4]. When properly designed, such wrap-faced GRS walls are also noted to perform better under seismic action [5], whose responses have been investigated using various methods, including experimental studies conducted with shake tables [6-9], analytical approaches such as pseudo-static and pseudo-dynamic analyses [10-11], and numerical modeling techniques using finite element and finite difference methods [12-16] mentioned that only a limited number of numerical analyses have been performed to predict the performance of wrap-faced GRS walls. Hence, in such case, numerical modeling is particularly valuable for simulating large-scale prototypes that are practically taxing to conduct regular tests in the laboratory.

GRS wall consists of four main components: the reinforced backfill, the retained fill, the facing

component, and the reinforcements. Granular backfill soils are recommended in GRS wall due to their excellent drainage properties and high shear strength, ensuring optimal wall performance. According to the Federal Highway Authority guideline FHWA-NHI-10-025 [17], British Standard code BS8006-1 [18] and Indian Roads Congress IRC SP102 [19], coarser materials with less than 15% fines and 6% plasticity index (PI) are ideal for backfill in GRS walls. The National Concrete and Masonry Association (NCMA) guideline [20] allows up to 35% of fines in a backfill material. Backfill material comprising fines beyond the above-mentioned ranges is termed as 'marginal backfill soils'. In the hilly and mountainous regions, the scarcity of granular materials presents logistical and cost challenges, leading to the increasing use of marginal soils as backfill. Many regions in India, including the north-eastern region, have an abundance of tropical soils that can be utilized as marginal soil fill. Marginal soils, though less ideal, offer significant economic and environmental benefits by reducing the CO_2 emissions associated with hauling of granular materials. Research studies demonstrate that transporting one ton of backfill generates 197.2 g of CO_2 per kilometer, while excavation and loading add an additional 0.386 kg per ton [21-22].

Quite a few researchers have worked on experimental and numerical fronts in assessing the response of GRS walls with marginal or cohesive backfills. Liu *et al*. [23] reported the use of higher reinforcement stiffness in marginal soil backfilled GRS wall that resulted in the reduction of the long-term relative creep of reinforcements and backfill. Balakrishnan and Viswanadham [24] reported that GRS walls constructed with marginal backfill and stronger equal-length geogrid layers exhibit minimal surface settlement, face movement, and peak strains in reinforcement layers. Rigorous shake table tests conducted on modular block-faced GRS walls with marginal backfill revealed that such walls can endure intense shaking without any stability issues or signs of imminent failure. The maximum deformations observed in such test models with cohesive backfill were found to be less than half of those obtained in the sand-filled models [25]. Chehade *et al*. [10] conducted pseudo-dynamic analysis of GRS wall with cohesive backfill soil and investigated the influence of horizontal and vertical acceleration coefficients (k_h and k_v) on the internal seismic stability of GRS wall with tension cracks in the backfill material. The output showed that an increment in the soil strength parameters reduces the requirement of a reinforcement with higher tensile capacity. Li and Yang [26] conducted seismic analysis of GRS wall with cohesive backfill having tension cracks. The aim of the study was to assess the minimum

tensile strength of reinforcement that is required to prevent failure, determined through a combination of kinematic limit analysis and pseudo-dynamic loading. The output depicted that a small increase in backfill cohesion significantly reduces the required reinforcement tensile strength. It was also observed that a pseudo-dynamic analysis yielded less conservative estimates when no amplification was considered.

The present study aims to investigate seismic response wrap-faced GRS wall with marginal backfill. Static and pseudo-static response of GRS wall is also presented as benchmark analyses. The study aims to develop a comprehensive understanding of the failure mechanisms, deformation patterns, and stress distribution in GRS walls with marginal backfills subjected to seismic loading. Based on the variations in reinforcement stiffness and backfill cohesion, the study explores the behaviour of the GRS wall response of lateral wall face displacement, mobilized reinforcement load, mobilized reinforcement strain, acceleration amplification and potential failure surface..

2. NUMERICAL MODELING OF WRAP-FACED GRS WALL

2.1. Finite Element Modeling

A two-dimensional finite element (FE) model is developed to study the seismic performance of a wrap-faced GRS wall with the aid of RS2 module of Rocscience FE package (v11.024). The FE model corroborates to a wrap-faced GRS wall constructed to safeguard an important building structure located at the North East Police Academy (NEPA) in Shillong, Meghalaya, India. The wall has a height of 6 m with a vertical face (without any batter angle). The backfill material is considered placed at equal lifts of 0.3 m. The foundation of the model wall is considered extended up to 10 m below the wall base. Geotechnical investigation of the virgin foundation soil material from the worksite was carried out. The foundation soil is found to be having a unit weight (γ_f) of 22.6 kN/m³, internal friction angle (φ_f) of 39°, cohesion (c_f) of 176.58 kPa, and modulus of elasticity (E_f) of 80 MPa; the same properties have been used as input to the FE model. Geotextile layers are used as primary reinforcement, which also acts as a wraparound face for each lift with a wrap tail length of 0.6 m. As reported by Kilic *et al.* [25], to safely support a marginal backfill, the length of reinforcement should prevail within the range 0.6H-0.8H, where H is the height of the GRS wall. In accordance, in the present study, a 4.2 m length of reinforcement (*i.e.*, 0.7H) is used both at the worksite as well as in the FE model, as shown in Fig. 1.

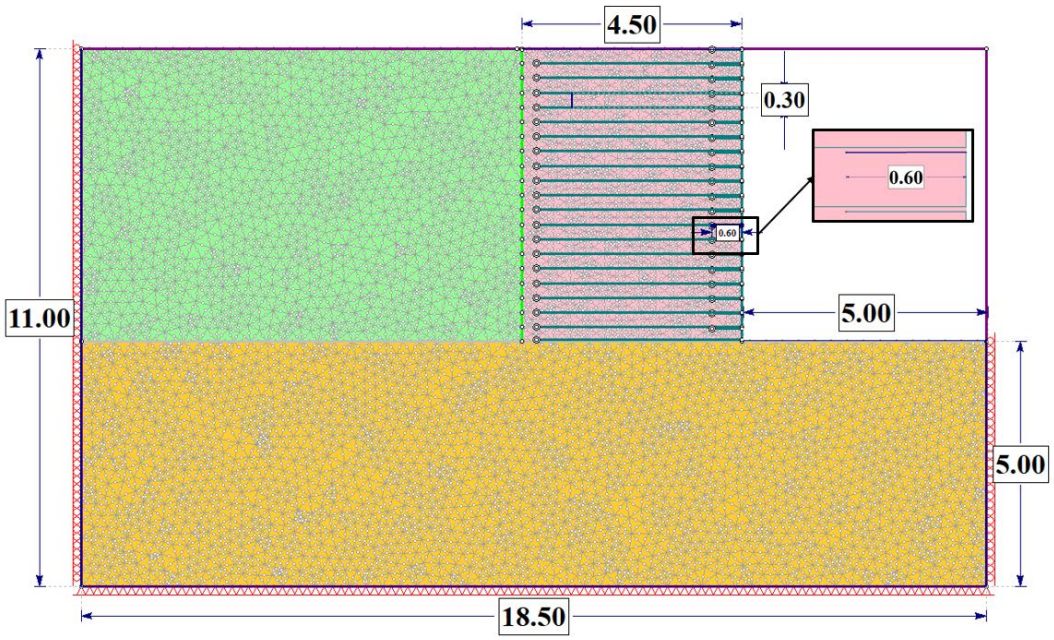

Fig. 1. Finite element model of wrap-faced GRS wall considered in the present study (all dimensions are in m)

2.2. Reinforced Backfill and Retained Fill Material Properties

As mentioned earlier, soils having percentage fines greater than 15% and PI > 6 qualify as marginal soils [17]. The particle size distribution assessment of the soil material used as reinforced backfill in the present study revealed percentage fines greater than 15% and a PI > 6, therefore qualifying it as a marginal material [27]. Laboratory geotechnical investigations indicated the marginal material to be having a unit weight (γ_b) of 18 kN/m^3, angle of internal friction (φ_b) of 44°, Poisson's ratio (v_b) of 0.3 and Young's modulus (E_b) of 15 MPa. To investigate the influence of backfill marginality on the response of the GRS wall, the backfill cohesion (c_b) was varied from 5 kPa to 16 kPa. This approach follows the earlier study by Majumder *et al.* [28], which examined the effectiveness of marginal fills with higher cohesion. Further, geotechnical investigation of the retained fill material exhibited a unit weight (γ_r) of 17 kN/m^3, internal friction angle (φ_r) of 30°, cohesion (c_r) of 1 kPa, a Young's modulus (E_r) of 15 MPa, and a Poisson's ratio (v_r) of 0.3. Both the reinforced backfill and retained fill soils are modelled as Mohr-Coulomb material following non-associated flow rule in which no dilation is considered. Further, it is to be noted that the entire analysis reported herein have considered the reinforced backfill and retained fills to be in dry state without incorporating any hydraulic conditions.

2.3. Geotextile Reinforcement

The geotextile reinforcement is modelled using isotropic linear-elastic 'geosynthetic liner' elements in Rocscience RS2 (v11.024). The geosynthetic elements are modeled as two-noded linear elements, capable of carrying axial tensile forces. To account for the installation damage and durability, the ultimate tensile strength (T_{ult}) obtained from high-rate tensile loading tests of virgin specimens are lowered to the design strength (T_d) with the aid of corresponding reduction factors for installation damage and durability (RF_{ID} and RF_D). The design strength (T_d) is further adjusted for creep effects to obtain the unfactored design strength (T_{do}) with the aid of corresponding reduction factor (RF_{CR}) that reflects the field conditions under sustained static loads. Finally, T_{do} is divided by the overall safety factor $(F_s)_{overall}$, which includes both material and structural safety factors, to arrive at the long-term tensile strength (T_{LTS}) of the geotextile reinforcement [1], and the same can be calculated from Equation (1) and Equation (2) as follows:

$$T_{do} = \frac{T_{ult}}{RF_{ID} \times RF_{CR} \times RF_D} = \frac{T_d}{RF_{CR}} \quad (1)$$

$$T_{LTS} = \frac{T_{do}}{(F_s)_{overall}} \quad (2)$$

In this particular study, three different types of geotextile reinforcement are considered, namely Wavin TR5000 HF, Wavin TR7000 HF, and Wavin TR10000, having the tensile stiffness (E_R) of 810 kN/m, 1051 kN/m and 1420 kN/m, respectively, and ultimate tensile strengths (T_{ult}) of 90 kN/m, 140 kN/m, and 220 kN/m, respectively. The analysis considered a creep reduction factor (RF_{CR}) of 1.6, an installation damage factor (RF_{ID}) of 1.05, a deterioration in service factor (RF_D) of 1, and an overall factor of safety $(Fs)_{overall}$ of 1.05. The properties of geotextile used in present study is listed in Table 1.

Table 1: Geotextile reinforcement properties as used in the present study

Reinforcement type	Tensile stiffness E_R (kN/m)	Long-term tensile strength T_{LTS} (kN/m)
Wavin TR5000 HF	810	51
Wavin TR7000 HF	1051	79
Wavin TR10000	1420	125

2.4. Geotextile Reinforcement

Assessing the interface properties forms a crucial part as a proper interface modelling guides the response of GRS walls through FE simulations. The soil-geotextile interface interaction can be determined in the laboratory using direct shear or pull-out tests. The interaction mechanism between geotextile and marginal fill soils have been successfully conducted through pull-out tests by earlier researchers [29-31]. In the present study, the interface system is modeled using 'joint' property in RS2, in which the interface between the geotextile and backfill soil material is modeled by Mohr-Coulomb (M-C) criteria that is described by the interfacial adhesion (c_{ai}) and angle of interface friction (δ_i). Further, to describe the slippage of soil-geotextile interface, the shear stiffness (k_s) and normal stiffness (k_n) are assessed as inputs. The peak interface friction angle (δ_i) is taken as 44°, the peak interface adhesion (c_{ai}) as 2.5 kPa, the shear stiffness (k_s) as 10 MPa/m/m, and the normal stiffness (k_n) as 100 MPa/m/m [32].

2.5. Meshing and Boundary Conditions

In the present study, 6-noded triangular elements are used to create the mesh to discretize the developed FE model. Meshes with coarser sized elements fail to capture the accuracy of the responses, while too finer mesh lead to increment of computational cost and accumulation of integral errors. Hence, in the present study, the balance is achieved by discretizing the model with an appropriate number of 4000 elements. Furthermore, at appropriate locations within the FE model, e.g. locations expected of stress and strain concentrations, mesh refinement is carried out, leading to a total of 8755 elements discretizing the entire FE model.

Defining boundary conditions forms an inevitable part of the FE model development. In the present study, for the static and pseudo-static analyses, the far lateral boundaries of the FE model have been provided with roller connections that restrict it from displacing in horizontal directions while permitting to move in vertical direction to allow the possible settlements. Further, the bottommost part of the model has been provided with a fixities that restrict movement in both vertical and horizontal directions. The topmost layer of the retained fill and the GRS wall, as well as the face of the wall, is free to displace and, hence, is devoid of any boundary fixities. In the case of dynamic analysis, transmitting boundary conditions are applied to the left and right vertical faces of the wall to allow earthquake waves to enter the model, while absorbent boundary conditions are imposed

at the base to dissipate incoming waves and prevent reflection back into the model. A Rayleigh damping of 2% is used for conducting the dynamic analysis.

2.6. Input Strong Motion

In the present study, the seismic analysis of the wrap-faced GRS wall with marginal backfill soil is conducted by subjecting it to the 1995 Kobe motion recorded at the Kakogawa (CUE90) station on January 16, 1995. Based on the same input motion, pseudo-static analyses conducted for the present study also uses the peak horizontal acceleration (PHA) of 0.344g. Fig. 2 shows the acceleration-time history for Kobe earthquake motion that is applied at the base of the FE model, along with its frequency domain decomposition. Table 1 provides the important strong motion characteristics of the chosen input motion.

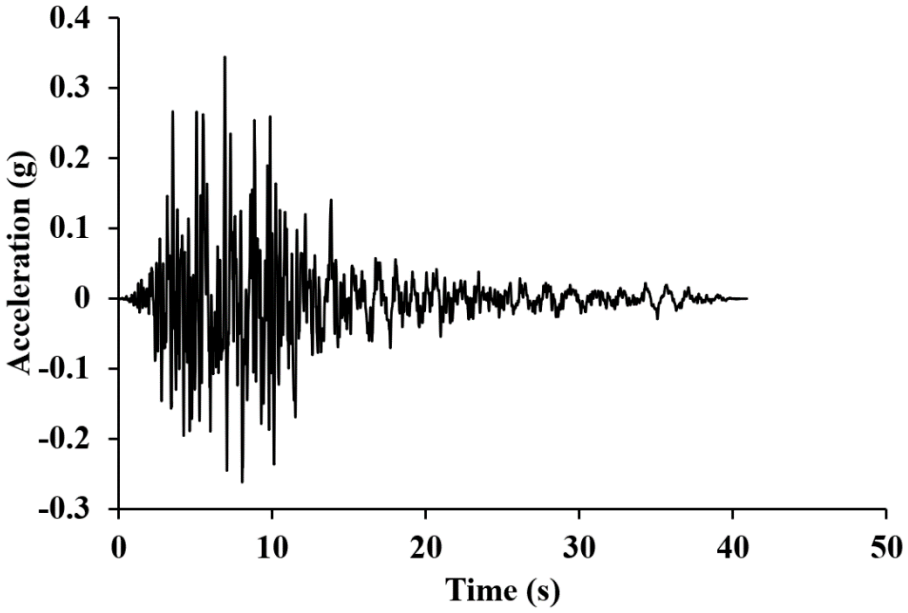

(a)

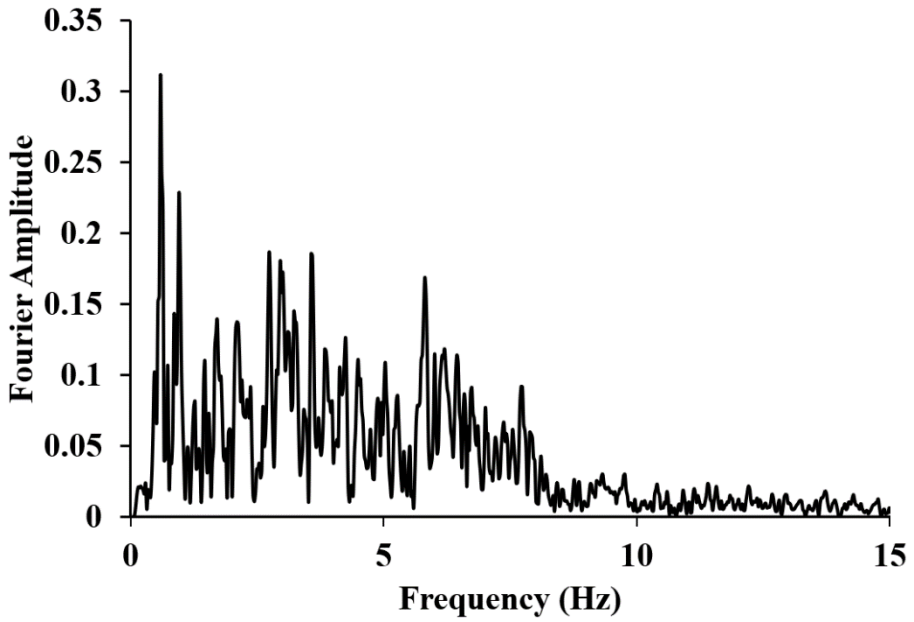

(b)

Fig. 2. Strong motion signature of the 1995 Kobe motion (a) Acceleration-time history (b) Frequency-domain response

Table 1 Strong motion characteristics of the 1995 Kobe earthquake motion

Parameter types	Parameter	Values
Amplitude Parameter	Peak Acceleration (g)	0.34
	Peak Velocity (cm/s)	27.68
	Peak Displacement (cm)	9.69
	Acceleration RMS (g)	0.05
	Arias Intensity (m/s)	1.69
	Specific Energy Density (cm^2/s)	1625.94
	Sustained Maximum Acceleration (g)	0.27
Frequency parameters	Predominant Period (s)	0.16
	Mean Period (s)	0.54
Duration Parameter	Time of Peak Acceleration (s)	6.93
	Time of Peak Velocity (s)	5.84
	Time of Peak Displacement (s)	11.41

3. VALIDATION AND VERIFICATION STUDY

A validation study is conducted in regard to the performance of full-scale wrap-faced geosynthetic reinforced soil (GRS) walls using the experimental work reported by Yu *et al*. [16]. In the reported program, two 3.6 m high instrumented walls were constructed at the Royal Military College of Canada (RMCC). Although both walls had the same geometry and backfill soil, one was reinforced with a stiff welded wire mesh (WWM) while the other with a flexible biaxial polypropylene (PP) geogrid. The walls, each 3.6 m high and 3.4 m wide at the face, were built using a wrap-faced technique, with the reinforced soil zone plus backfill extending 5.65 m behind the wall as shown in Fig. 3. Among the two walls, the one reinforced with PP geogrid is chosen for the present validation study. Six layers of reinforcement were are used at a vertical spacing of 0.6 m, wherein each reinforcement layer forms a wraparound over the sand backfill with a wrap tail length of 0.6 m. It is to be noted that the sand backfill was compacted in four numbers of 0.15 m lifts within each of the geotextile wraparounds. The study evaluated vertical stresses at the base of GRS wall, the axial strains in each reinforcement layer and the peak tensile load in the reinforcements embedded within the backfill.

Yu *et al*. [16] also developed a numerical model of the GRS wall with the aid of the finite difference package, FLAC 2D. The numerical model explicitly represented the soil, reinforcement layers, and facing wraps as has been used in the experimental model. The backfill soil, having a unit weight of 16.8 kN/m^3, was modeled using of a linear elastic-plastic model (with Mohr-Coulomb failure criterion). The backfill zone had a Young's modulus of 80 MPa, Poisson's ratio of 0.3, peak friction angle of 44°, dilation angle of 11°, and cohesion of 1 kPa. Within the facing zone, the backfill was considered to be devoid of cohesion and dilation with a reduced magnitude of Young's modulus of 20 MPa and a residual friction angle of 35°. The PP geogrid reinforcement was modeled using cable elements with initial tangent stiffness of 122 kN/m and ultimate tensile strength of 14 kN/m, obtained from laboratory tensile and creep tests, respectively. The concrete foundation was modeled as a linear elastic material with a Young's modulus of 32 GPa, Poisson's ratio of 0.15, and unit weight of 22.9 kN/m^3. The interface between concrete and soil was considered to have a friction angle of 44°, dilation angle of 11°, adhesion of 1 kPa, normal stiffness of 100 MPa/m, and shear stiffness of 10 MPa/m. Following the same parameters prescribed by Yu *et al*. [16], Sharma and Prashant [15] developed a two-dimensional plane strain FE model of the

same wrap-faced GRS wall using GiD v11 and OpenSees v2.5. The developed numerical model was validated by comparing its predictions of facing deformation profiles and peak reinforcement force profiles and with the corresponding experimental measurements by Yu *et al*. [16].

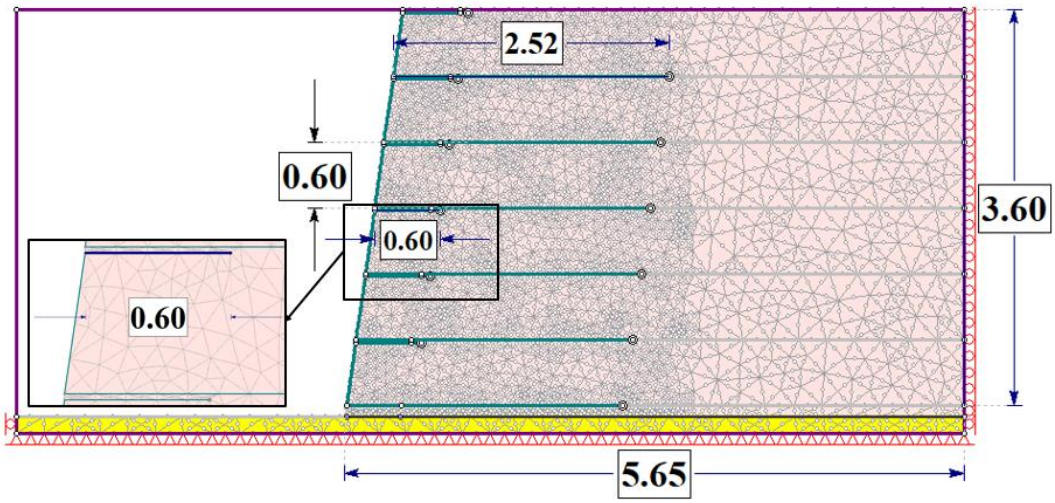

Fig. 3. Finite element model of the wrap-faced GRS wall used for the validation study (all dimensions are in m)

Following the details provided by Yu *et al.* [16], in the present validation-cum-verification study, the finite element model of the GRS wall with flexible biaxial polypropylene (PP) geogrid is developed in RS2. The outcomes of the present study, in terms of the vertical stresses on the foundation and reinforcement loads are compared with the previous studies. Fig. 4 and Fig. 5 present the vertical stresses at the base of the wall, normalized by (unit weight of backfill × wall height), and profile of the peak reinforcement force at each layer, respectively, obtained from the present study. As can be observed from the figures, the predictions from the present numerical analysis are found to be in reasonable agreement with the experimental findings by Yu *et al*. [16] and are in excellent agreement with the numerical findings reported by Yu *et al*. [16] and later by Sharma and Prashant [15]; rather the present numerical findings are observed to be in better agreement than that reported by Sharma and Prashant [15].

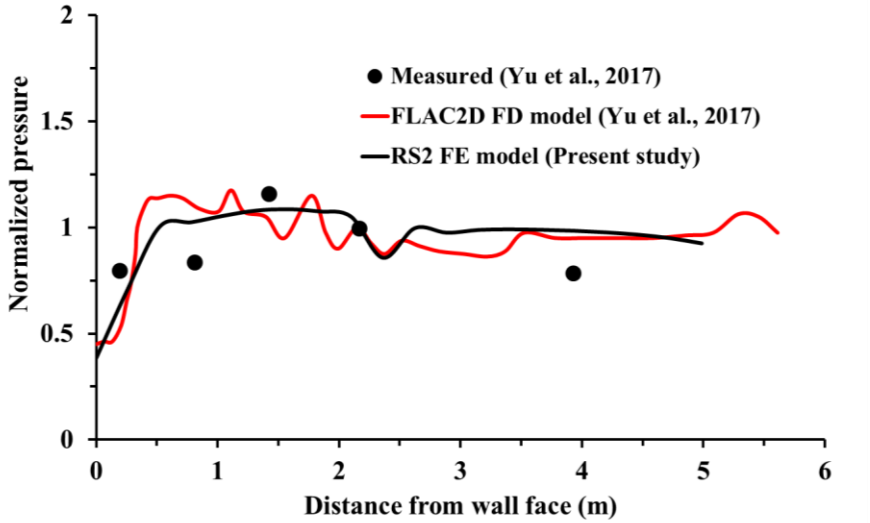

Fig. 4. Validation and verification of the vertical stress distribution at the base of the geogrid wrap-faced GRS wall

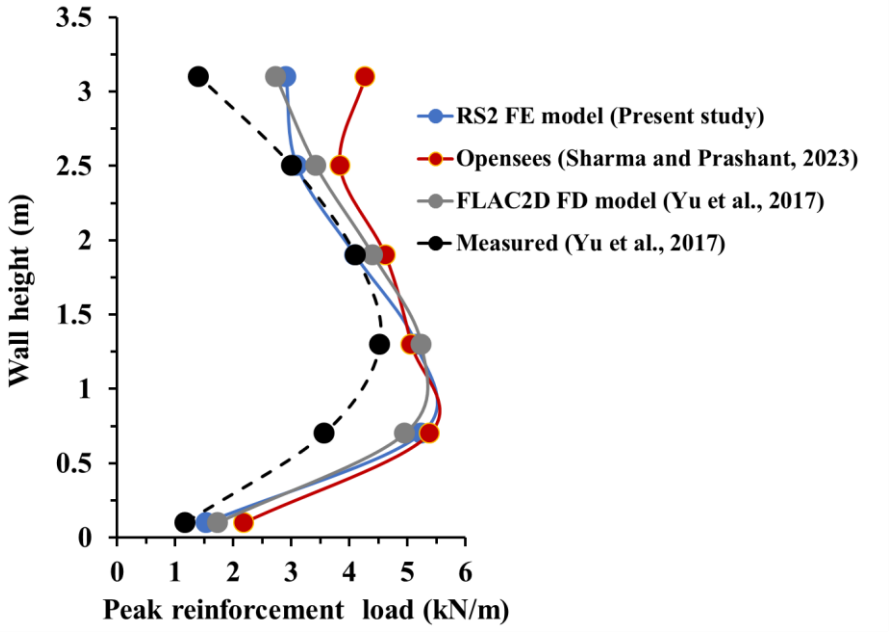

Fig. 5. Validation and verification of the peak reinforcement load profile for geogrid wrap-faced GRS wall

4. RESULTS AND DISCUSSIONS

As per the standard guidelines, a granular backfill is an ideal choice for a GRS wall. However, as described earlier, the use of marginal soils as a backfill in the GRS walls have gained popularity out of the necessity. Given such a situation, it is important to understand the influence of that specific parameter that transduces the soil to be marginal, i.e. backfill cohesion. Further, it is well established that the reinforcement stiffness plays an influencing role in the altering the response of GRS walls when a granular backfill is used. It would be interesting to note that if there is a similar influence when the backfill turns out to be marginal. Hence, in the present study, the response of a GRS wall is discussed due to simultaneous variations in the backfill cohesion (5 kPa, 10 kPa and 16 kPa) and reinforcement stiffness (as mentioned in Table 1). It is to be noted that all the reinforcements of the GRS wall are considered of same length and stiffness for a given model representation.

4.1. Stability of the GRS Wall with Marginal Backfill under Static, Pseudo-Static and Dynamic Loading Scenarios

The present study mainly focuses on the response of the wrap-faced GRS wall with marginal backfill soils under dynamic conditions. In this context, as a benchmarking, static and pseudo-static analyses are also conducted to understand the corresponding stability aspects, and assess their differences with that obtained from subsequent dynamic analysis. Figure 6 shows the influence of backfill cohesion and reinforcement stiffness on the vertical displacement contours of the GRS walls under static condition. It can be noted that for all the combination of the influencing parameters, two distinct zones of vertical displacement are formed in the GRS wall: one in the reinforced backfill and the other in the retained fill. A distinct triangular wedge is formed in the retained fill for each case; however, the magnitude of deformation within the contour zone increases with an increase in c_b and a decrease in E_R. The retained soil exhibits wider zones of deformation when the c_b is larger, which is attributed to the effect of backfill cohesion on soil–reinforcement interaction within the reinforced fill. With an increase in c_b, the soil-reinforcement interaction is reduced, allowing higher relative displacement in the reinforced backfill and, subsequently, more profound vertical deformation contours in the retained fill. Conversely, with an increase in E_R, the reinforcement becomes stiffer and more effective in controlling lateral

displacement, leading to a significant reduction in both the magnitude and extent of vertical deformation within the retained fill. Importantly, the inclination angle of the contours remains unchanged, indicating that the overall failure mechanism and geometry of the deformation wedge are not altered, but the severity and spread of deformation are strongly influenced by the combined effect of c_b and E_R.

Further, it is noticed that the angle of vertical displacement contours in the retained fill zone is nearly 45°. With the friction angle of the retained fill being 30°, according to Rankine's active earth pressure theory, if the retained fill is subjected to active failure without any GRS wall support, the inclination of the failure plane would be approximately $(45 + \varphi_r/2)$, i.e. 60° with the horizontal. However, the present analysis shows a much flatter inclination of about 45°, which deviates significantly from the theoretical prediction. This difference indicates the restraining influence of the GRS wall system. The reinforcement layers reduce the lateral soil movement and redistribute stresses within the retained fill. Consequently, the deformation contours do not follow the classical active failure pattern, rather flatten out due to the confining and reinforcing effects of the wall. This implies that the GRS wall alters the natural failure mechanism by reducing mobilized shear strains and enhancing stability, leading to a modified deformation profile that is governed more by soil-reinforcement interaction than by soil shear strength alone.

The displacement contours within the reinforced backfill are observed to extend until the bottom of the wall, which is expected, since the entire wrapped fascia undergoes outward displacement. With a decrease in the backfill cohesion (c_b) and an increase in the reinforcement stiffness (E_R), both the extent and magnitude of the displacements are considerably reduced. The reinforcement layers play a crucial role in confining soil movement, thereby restricting the outward spread of displacements toward the fascia. Unlike the retained fill, which develops a triangular wedge-shaped deformation pattern typical of a homogeneous soil mass, the reinforced backfill exhibits a distinct bilinear contour pattern. This bilinear nature arises due to soil-reinforcement interaction: one zone is influenced primarily by the outward displacement of the fascia, while the other is controlled by the anchorage and confinement imparted by the reinforcement layers. The transition between these two zones gives rise to the bilinear form, which highlights the efficiency of reinforcement in redistributing stresses and controlling deformations throughout the backfill. This

makes the deformation mechanism of the reinforced backfill fundamentally different from that of the retained fill and clearly demonstrates the stabilizing effect of reinforcement.

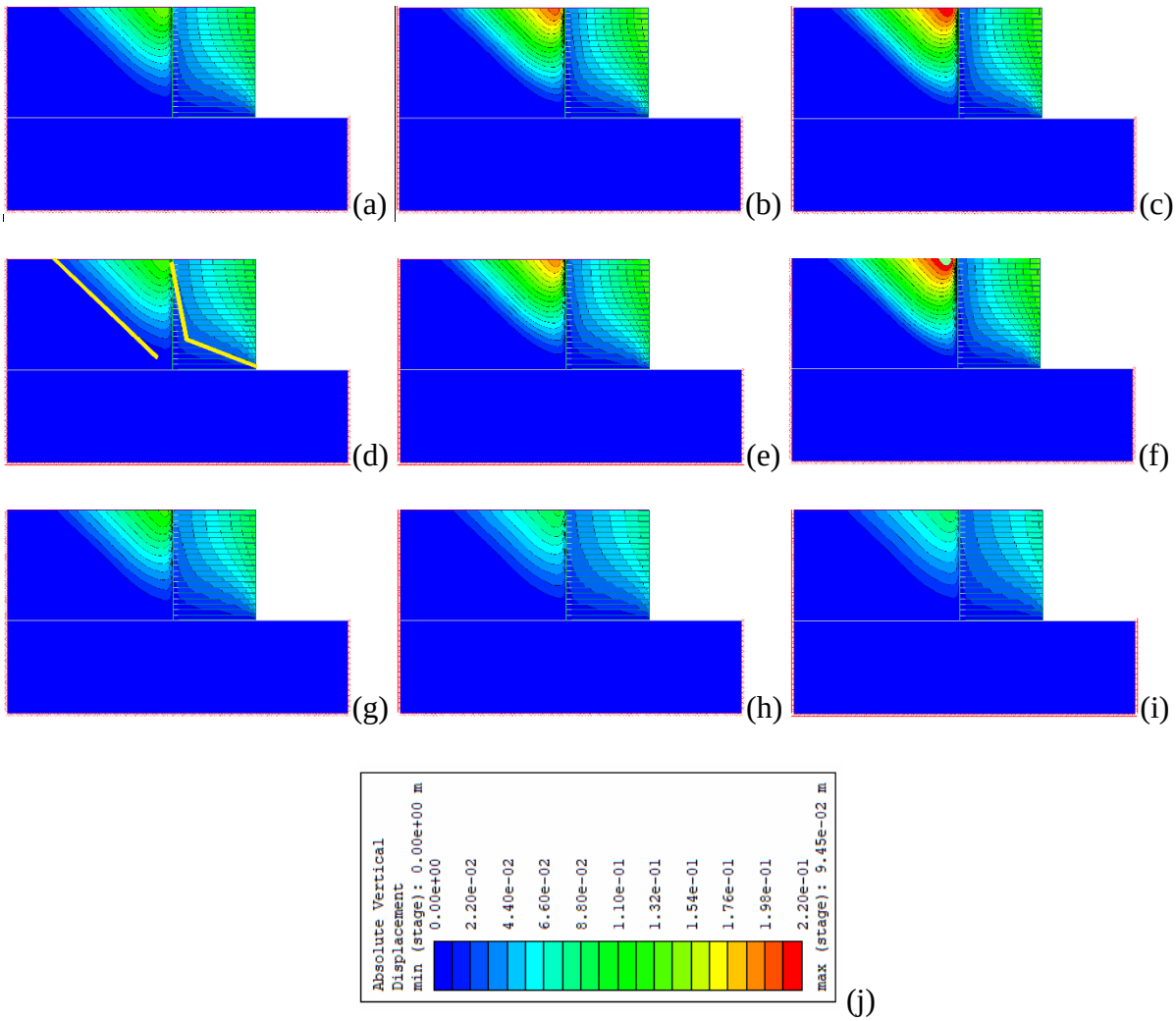

Fig. 6. Vertical displacement contours of the wrap-faced GRS wall under static analysis (a) c_b = 5 kPa, E_R = 810 kN/m (b) c_b = 10 kPa, E_R = 810 kN/m (c) c_b = 16 kPa, E_R = 810 kN/m (d) c_b = 5 kPa, E_R = 1051 kN/m (e) c_b = 10 kPa, E_R = 1051 kN/m (f) c_b = 16 kPa, E_R = 1051 kN/m (g) c_b = 5 kPa, E_R = 1420 kN/m (h) c_b = 10 kPa, E_R = 1420 kN/m (i) c_b = 16 kPa, E_R = 1420 kN/m (j) vertical displacement contour legends

The maximum shear strain contours are presented at the critical stability stage for static and pseudo-static analyses, illustrating the influence of cohesion (c_b) and reinforcement stiffness (E_R), as shown in Fig. 7 and Fig. 8, respectively. The changes of the contour magnitude increments and

decrements are consistent with that discussed for the vertical displacement contours. Reinforcement stiffness has a more pronounced effect on reducing both the vertical displacement and the maximum shear strain magnitudes in the retained fill and reinforced fill zones. Due to the stiffness contrast between the reinforced and retained fill, the maximum shear strain band is mobilized at the interface and extends into the retained fill. However, the presence of reinforcement within the reinforced zone distributes the shear stress more evenly, preventing a distinct shear strain band from developing in this region. The backfill cohesion (c_b) exerts a stronger influence on increasing the stability compared to reinforcement stiffness (E_R).

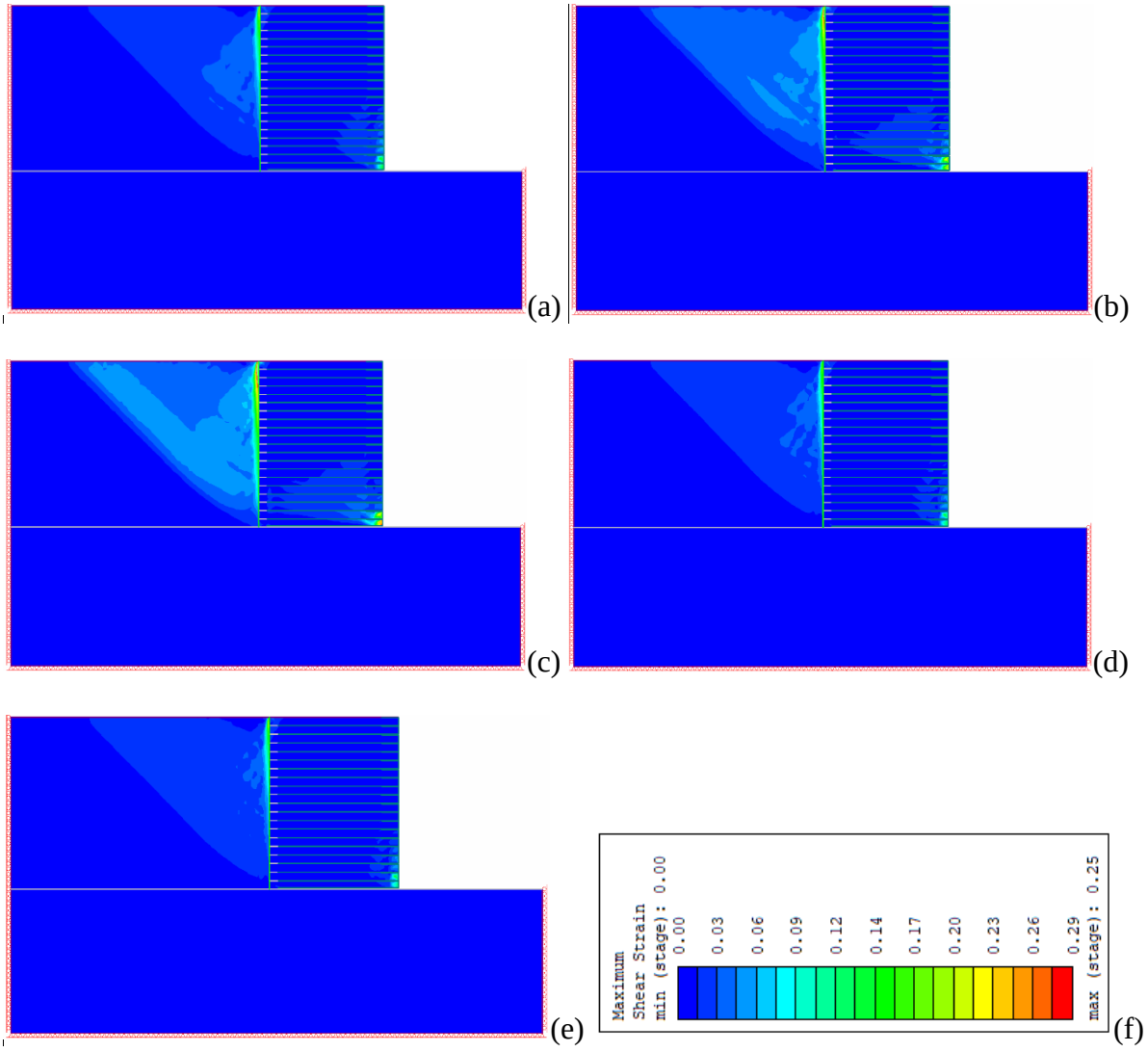

Fig. 7. Maximum shear strain contours under static analysis: (a) c_b = 5 kPa, E_R=810 kN/m (b) c_b = 10 kPa, E_R =810 kN/m (c) b) c_b = 16 kPa, E_R =810 kN/m (d) c_b = 5 kPa, E_R =1051 kN/m (e) c_b = 5 kPa, E_R =1420 kN/m (f) maximum shear strain contour legends

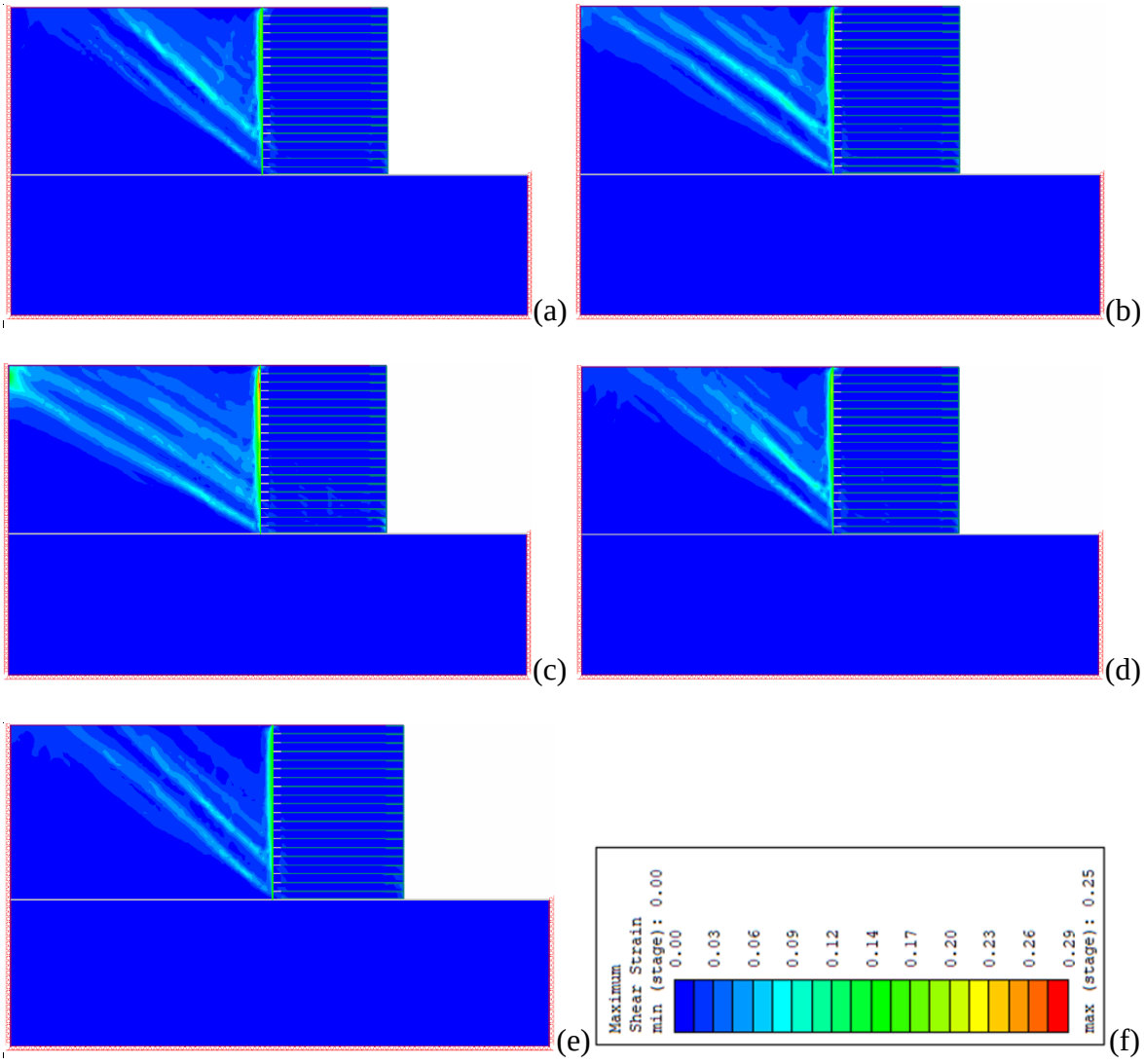

Fig. 8. Maximum shear strain contours under pseudo-static analysis: (a) c_b = 5 kPa, E_R=810 kN/m (b) c_b = 10 kPa, E_R =810 kN/m (c) b) c_b = 16 kPa, E_R =810 kN/m (d) c_b = 5 kPa, E_R =1051 kN/m (e) c_b = 5 kPa, E_R =1420 kN/m (f) maximum shear strain contour legends

From a finite element-based analysis, the stability of a GRS wall can be analyzed using the 'strength reduction technique' that culminates in the assessment of the strength reduction factor (SRF) [33] that is an equivalent to the factor of safety (FoS) found in the limit equilibrium analysis [34]. This involves an iterative reduction of the initially considered soil shear strength parameters by a certain factor until the GRS wall reaches a limiting state of failure. Firstly, the FE program assesses the stability of the GRS wall utilizing the initial shear strength parameters (c and φ). If the GRS wall is found to be stable, the initial shear strength parameters are reduced to new

magnitudes c^{Trial} and φ^{Trial} with the aid of a trial factor F^{Trial}, and stability of the GRS wall is further checked. This process is iteratively repeated with different magnitudes of adjusted F^{Trial} (as per Equations 3 and 4) until the limiting state of failure is reached. For each SRF trial increment, RS2 executes a finite element stress analysis and monitors the convergence. If the model is stable (i.e. it if converges), the SRF is increased, whereas if it fails to converge, the bracket is set between the last converged SRF and the first failed SRF. Thus, the SRF analysis method in the RS2 FEM follows a bracketing approach with incremental stepping and convergence checks.

$$c^{Trial} = \frac{c}{F^{Trial}} \tag{3}$$

$$\varphi^{Trial} = arctan\left(\frac{\tan\varphi}{F^{Trial}}\right) \tag{4}$$

The final magnitude of the trial factor which leads to achieving the limiting state of failure is considered as the critical SRF for the given GRS wall. As a typical example, Fig. 9 shows evolution of the trial SRF and the corresponding maximum total displacement of the model. It is to be noted that the displacements corresponding to the strength reduction technique are artefacts and has no direct bearing to the actual displacement undergone by the GRS wall with the actual (initial) shear strength parameters. It has only been used in this study for the sake of plotting the evolution of SRF. In this plot, the black markers exhibit the SRFs for which the FE model does not succumb to failure, while the red markers exhibit the SRFs for which the model fails i.e. the corresponding analysis does not converge to the numerical solution [35].

Figure 10 highlights the SRF obtained from static, pseudo-static and dynamic analyses of wrap-face GRS walls with varying backfill cohesion and reinforcement stiffness. The dynamic SRF is evaluated at the PGA of the input motion, corresponding to a time instant of 7 s. It can be seen that the magnitude of SRF is higher in the case of dynamic analysis compared with the benchmark (static) analysis. This increase can be accredited to the additional system stiffness mobilized under dynamic loading, where the repeated cyclic stresses enhance the interlocking between soil particles and reinforcement layers. The induced dynamic stresses promote a densification effect in the reinforced soil mass, which, in turn, improves its resistance to shear deformation. Moreover, the flexible nature of the GRS wall allows it to accommodate and redistribute the dynamic loads more effectively, thereby mobilizing greater confinement and reducing the extent of localized failure mechanisms. As a result, the system exhibits an improved overall stability response under dynamic

conditions, reflected in the higher SRF values when compared to static analysis. The results indicate that an increase in c_b leads to a consistent rise in SRF across all analyses, demonstrating the significant role of soil cohesion in improving system stability by reducing lateral earth pressure. In contrast, the influence of reinforcement stiffness (E_R) on SRF is found to be minimal, suggesting that cohesion governs the stability response more dominantly under all analysis conditions. Furthermore, it is illustrated that dynamic time-history analysis yields higher SRF values. Stress reversals, as observed under time-history analysis, can render stability to a GRS wall structure or can even lead to its failure because of stress accumulation. As observed in this study, the SRF under dynamic scenario indicates a more stable GRS wall structure that can be attributed to (a) the flexibility of the wraparound fascia GRS wall by itself exercises damping that aids in lessening of the dynamic effects and (b) the reduction of the dynamic effects due to the increased interfacial interaction marginal soil and geotextile reinforcement.

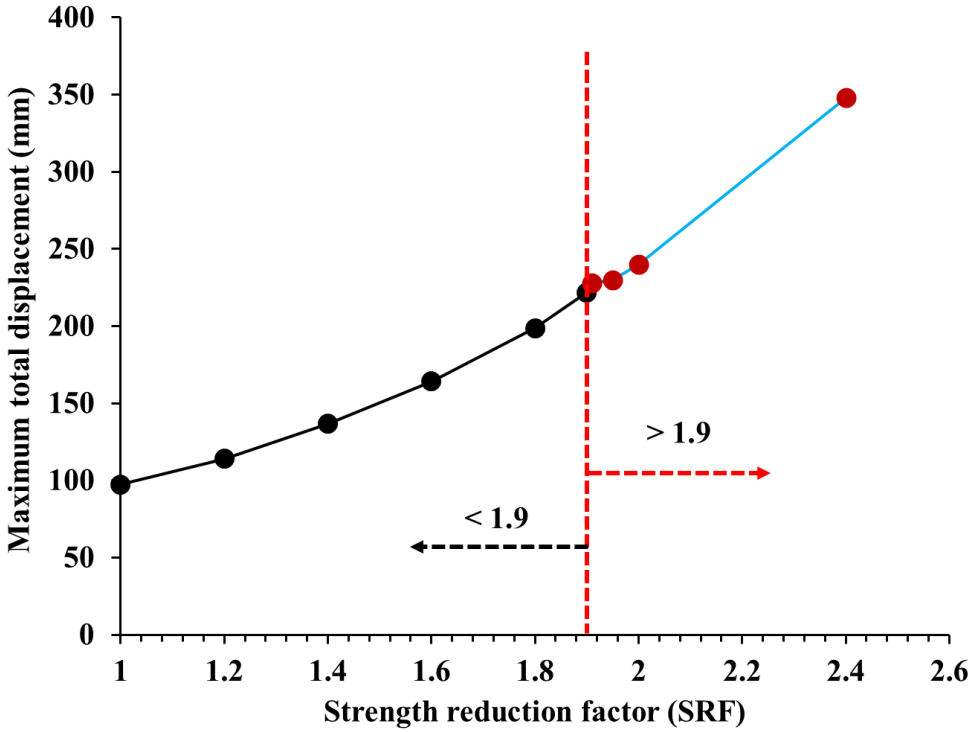

Fig. 9. Critical shear strength reduction factor for a typical wrap-faced GRS wall with c_b = 5 kPa and E_R = 810 kN/m

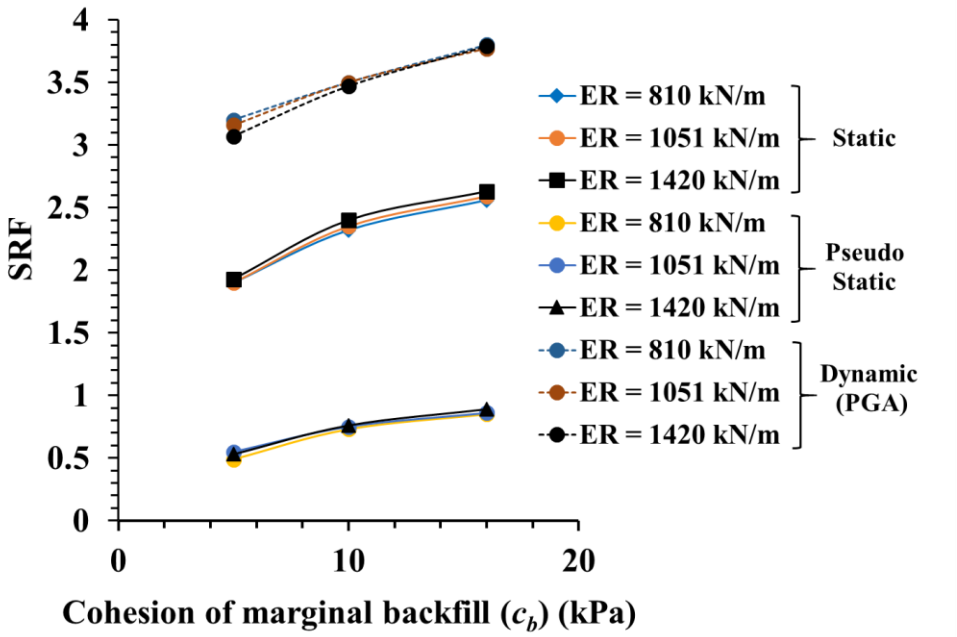

Fig. 10. SRF for varied cohesion of marginal soil and reinforcement stiffness

4.2. Lateral Face Displacement of GRS Wall with Marginal Backfill

The lateral face displacement of the GRS wall with marginal backfill under static, pseudo-static and dynamic conditions is computed for all the nine combinations of backfill cohesion and geotextile stiffness. Fig. 11 (a) illustrates a typical representation of the wall-face displacement, indicated with the aid of displacement vectors. Table 2 presents the peak displacement obtained from each of the cases. The results from the static analysis indicate that variation of both backfill cohesion and reinforcement stiffness have a negligible reduction effect on the in wall face displacement, the maximum change in displacement being 5 mm. This reduction is attributed to the enhanced shear strength provided by the cohesive soil and is in accordance to the established earth pressure theories highlighting the influence of backfill cohesion on the active earth pressure coefficient and active lateral stresses transferred on the retaining wall [36].

In comparison to the static response, the pseudo-static analyses resulted in a recognizably higher wall face displacement, which is attributed to the high additional pseudo-static force considered in the entire model. In contrary to the static response, the influence of backfill cohesion and

reinforcement stiffness are more prominent. For the same reinforcement stiffness, an increase in backfill cohesion have resulted in the increase in wall face displacement. This finding is in contrary to the conventional estimates of active earth pressure coefficient (K_a) in a standard gravity retaining wall with a cohesive-frictional backfill subjected to pseudo-static or pseudo-dynamic forces [36,37]. In such case, under limit equilibrium analyses scenarios, it is established that K_a decreases with the increase in backfill cohesion, thereby decreasing the lateral thrust on the wall face. However, in contrary to the rigid retaining walls for which the earlier findings are established, the GRS walls possesses substantial flexibility that can sustain more deformations and, hence, accommodate deformation-induced mechanisms and strength mobilizations. In this regard, an increase in the lateral stresses transferred to the wall under pseudo-static condition is noted in terms of the increased lateral displacement of the wall fascia. Further, it may be noted that the present study does to account any water-induced hydraulic scenarios and the marginal backfill is considered be completely dry. It is established by Lou *et al*. [38] that when water effects are not considered, marginal soil backfills with high cohesion exhibit brittle behavior at the micro-structural level. Once the cohesion bond is surpassed, the soil loses strength, leading to greater deformation. Additionally, marginal soils with high cohesion exhibit lower interface friction with geosynthetics compared to the granular soils with low cohesion. Consequently, due to the presence of fine particles, the mobilization of tensile forces at the soil-geosynthetic interface is hindered that reduces effectiveness of the reinforcement and results in higher wall face displacement with increase in cohesion. The above discussions are portrayed in Fig. 11 (b) through the variation in the fascia displacement of the wrap-faced GRS wall for various combinations of backfill cohesion and reinforcement stiffness. It can be noted that, in contrary to Fig. 11(a), Fig. 11(b) shows recognizable deviations in the wall-face displacement under various conditions as discussed, especially for c_b = 5 kPa while the difference in the fascia displacement profile decreases with the increase in backfill cohesion.

Fig. 11(c) highlights the fascia displacement of the wrap-face GRS wall under the chosen seismic motion. It may be noticed from Table 2 that the peak displacement from a nonlinear time-history analysis does not reflect a set pattern of variation with the changes in backfill cohesion. This is attributed to the fact that under the externally applied seismic inertial motion, the entire GRS wall system exhibits the development and evolution of seismicity induced stresses and strains over the

time as well; hence, the mobilized stresses are stated to evolve in both space and time. Consequently, a set pattern in the chance of evolution is not decipherable. However, it is well observed from Table 2 that the magnitude of the peak wall face displacement from the dynamic analysis is noticeably lesser than that obtained from the pseudo-static analysis, and the same is reflected in Fig. 11(c). This is attributed to the time-independent higher magnitude of lateral thrust transferred to the GRS system by considering the constant pseudo-static force to be 0.344g. However, for the dynamic analysis, the peak of the input motion (i.e. 0.344g) occurs only for a particular time-instant. As a result, the energy transferred by the time-dependent dynamic motion (proportional to the area under the input motion curve) is quite lesser than a constant pseudo-static scenario with 0.344g acting over the same time duration as that of the input motion. Further, owing to the stress reversals taking place in the dynamic motion, the lateral swinging motion developed in the wrap-faced GRS wall leads to energy dissipation. Additionally, higher strains induced in the GRS system under the dynamic condition also induces higher magnitudes of internal damping in the system [1]. In lieu of these developments, in comparison to pseudo-static responses, the maximum lateral displacement of the wall fascia is observed to be approximately 30%-50% lesser in case of dynamic analysis. The portrayal of the wall face displacement under the dynamic condition is illustrated in the Fig. 11(d). From the responses in each type of analyses and with marginal backfill having different cohesion magnitudes, it can be well noted that an increment of reinforcement stiffness lead to a reduction in the lateral displacement of the wall face that is attributed to the higher passive resistance induced by the geotextile reinforcement beyond the location of the potential failure plane.

Table 2 Maximum lateral displacement of the GRS wall face for varying reinforcement stiffness and backfill cohesion

Backfill cohesion (c_b) (kPa)	Maximum lateral displacement of GRS fascia (mm)								
	5			10			16		
Reinforcement stiffness (E_R) (kN/m)	810	1051	1420	810	1051	1420	810	1051	1420
Static analysis	66	64	64	64	63	62	62	62	61
Pseudo-static analysis	297	303	225	360	355	348	379	371	378
Dynamic analysis	205	208	187	194	208	202	206	202	200

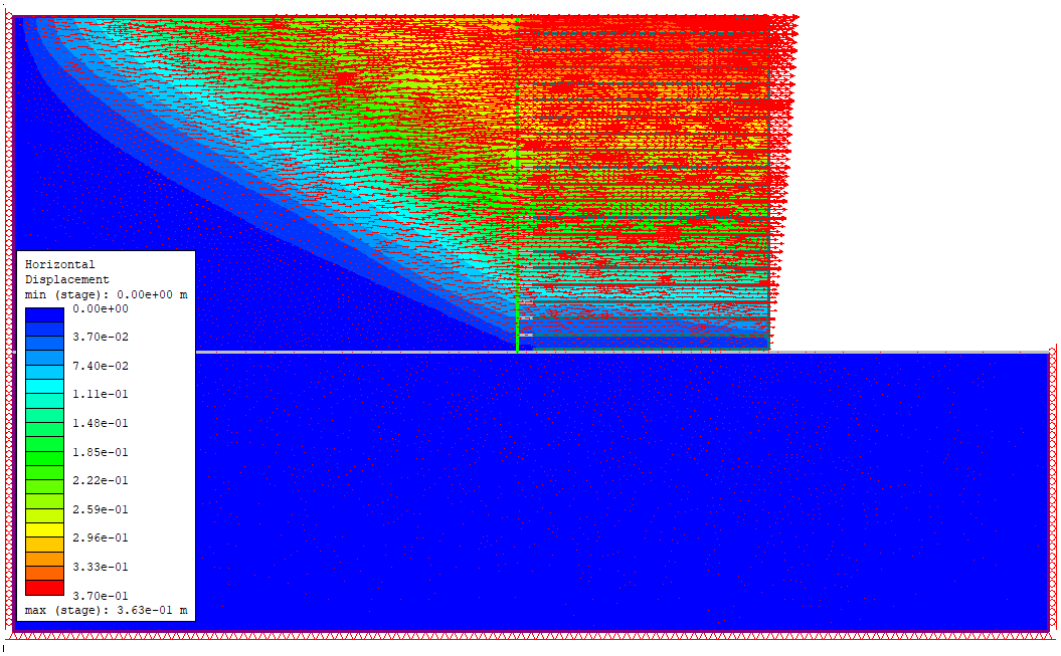

529 (a)

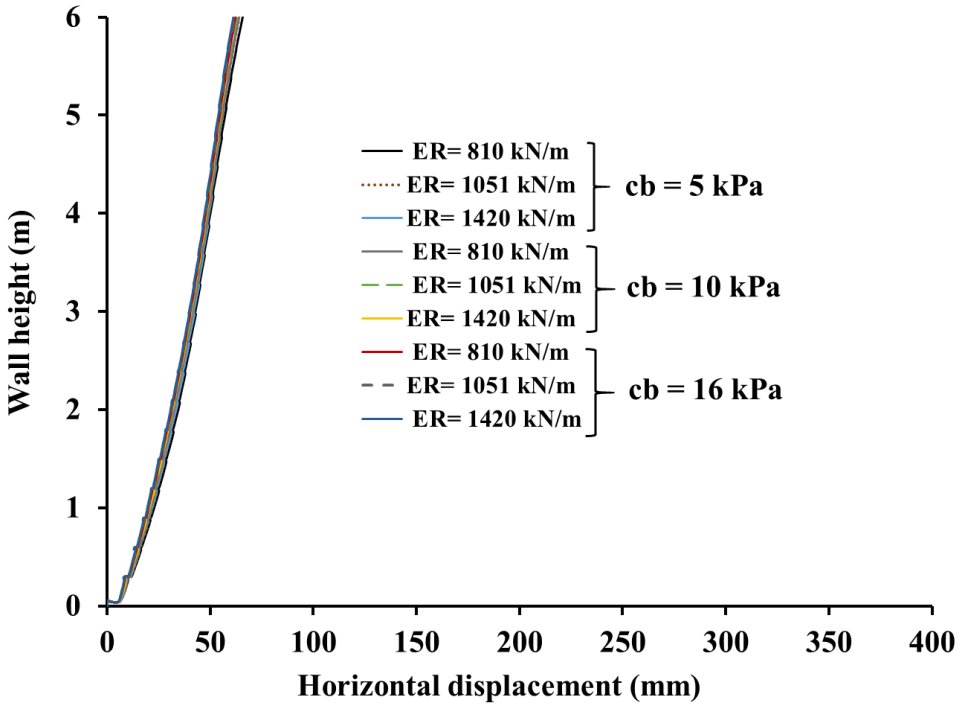

530

531 (b)

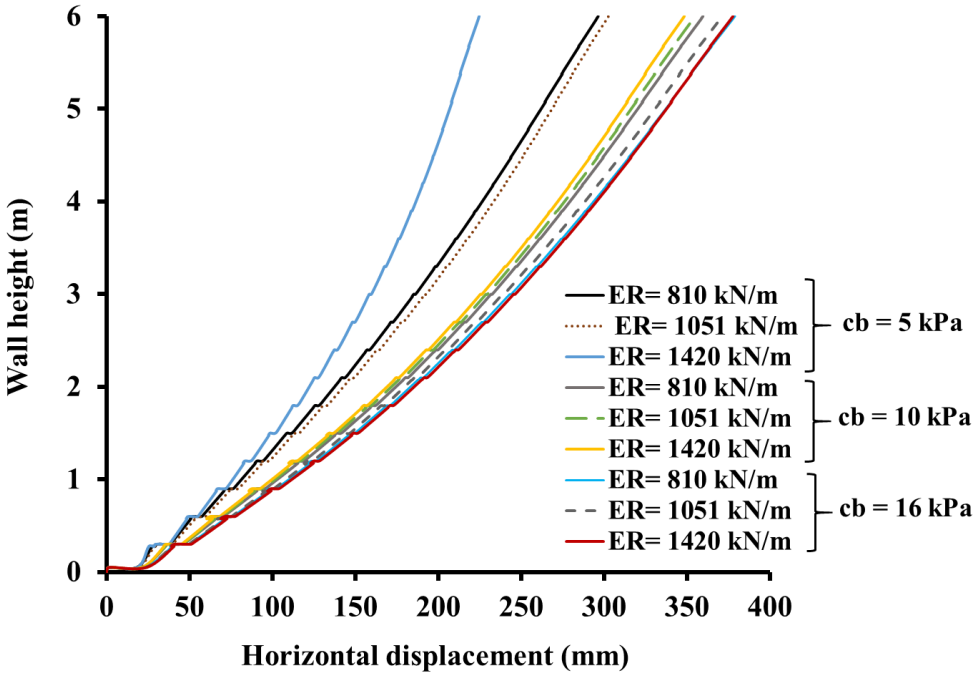

(c)

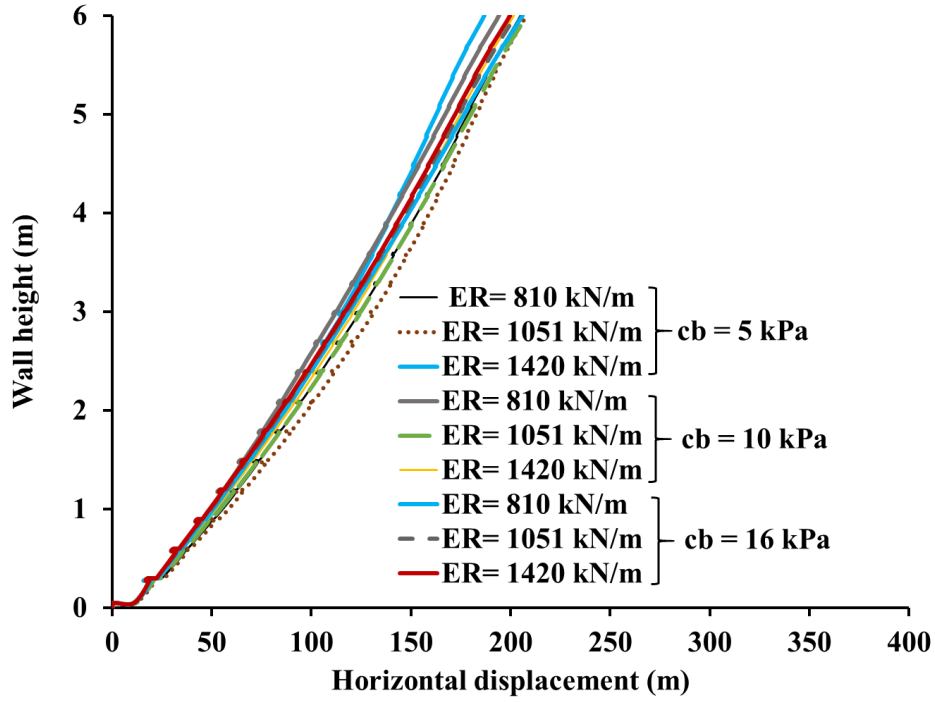

(d)

Fig. 11 Lateral displacement of the wrap-faced GRS wall highlighting (a) typical displacement vectors and observations from (b) static analysis (c) pseudo-static analysis and (d) dynamic analysis.

4.3. Mobilized Peak Reinforcement Load in GRS Wall with Marginal Backfill

Fig. 12 illustrates the profile of mobilized peak geotextile reinforcement along the wall height for varying backfill cohesion, reinforcement stiffness and analysis types. As noted earlier, under static analysis scenario, an increase in backfill soil cohesion results only in an insignificant reduction in mobilized reinforcement load, thereby indicating that the stress transfer mechanisms between the soil and geotextile reinforcement do not significantly alter under static conditions. In pseudo-static analysis, reinforcement load increases due to the additional seismic forces applied as inertial forces on the reinforced soil structure. These forces, represented by a seismic coefficient, increase the lateral earth pressure acting on the wall [39]. This results in higher mobilization of reinforcement load to resist the increased stresses. Marginal backfill soils, particularly those with higher cohesion, may exhibit brittle failure under combined static and seismic forces. Once the cohesion bond is overcome, the soil loses significant strength, increasing the dependence on the reinforcement for stability. Moreover, the seismic forces act as an acceleration multiplier, simulating amplified inertial effects, which further escalate the stress levels and load mobilization in the reinforcement.

In the dynamic analysis, a substantial reduction in reinforcement load mobilization is observed with increasing soil cohesion. This reduction is attributed to the behavior of cohesive soils, which exhibit the ability to dissipate dynamic loads over repeated loading cycles [1,40]. Additionally, the interaction at the soil-geotextile interface plays a critical role, as the fine particles in cohesive soils can reduce interface friction and tension mobilization [41,42], further influencing the load transfer to the reinforcement under dynamic conditions. It is noted for all the cases of analyses that an increment in the reinforcement stiffness leads to a notable increase in the mobilized reinforcement load that eventually changes the wall face horizontal deformation pattern, which is in tune to the findings reported in existing literature [43].

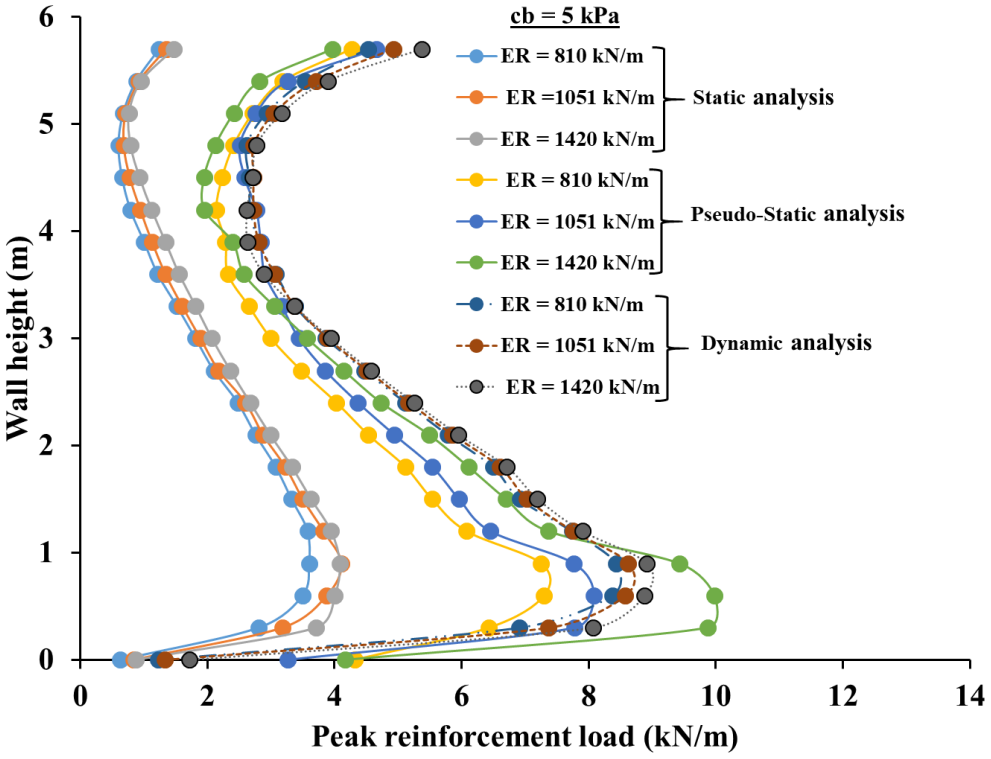
cb = 5 kPa
ER = 810 kN/m
ER =1051 kN/m
ER = 1420 kN/m
Static analysis
ER = 810 kN/m
ER = 1051 kN/m
ER = 1420 kN/m
Pseudo-Static analysis
ER = 810 kN/m
ER = 1051 kN/m
ER = 1420 kN/m
Dynamic analysis
Wall height (m)
Peak reinforcement load (kN/m)
0
1
2
3
4
5
6
0
2
4
6
8
10
12
14

565 (a)

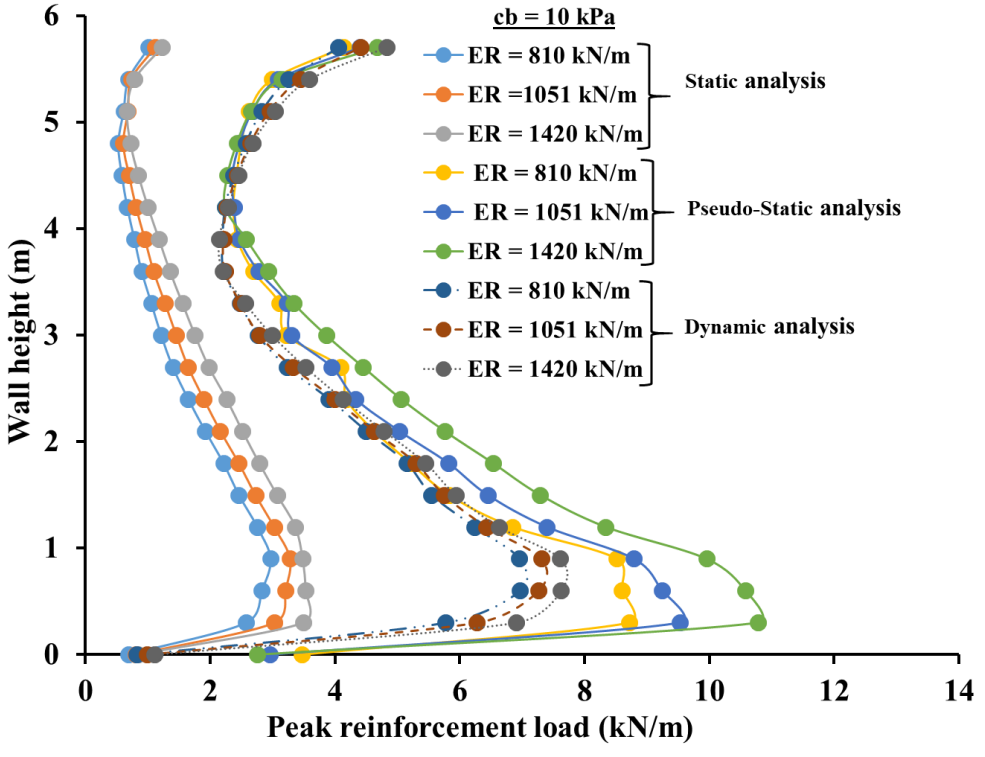
cb = 10 kPa
ER = 810 kN/m
ER =1051 kN/m
ER = 1420 kN/m
Static analysis
ER = 810 kN/m
ER = 1051 kN/m
ER = 1420 kN/m
Pseudo-Static analysis
ER = 810 kN/m
ER = 1051 kN/m
ER = 1420 kN/m
Dynamic analysis
Wall height (m)
Peak reinforcement load (kN/m)
0
1
2
3
4
5
6
0
2
4
6
8
10
12
14

566 (b)

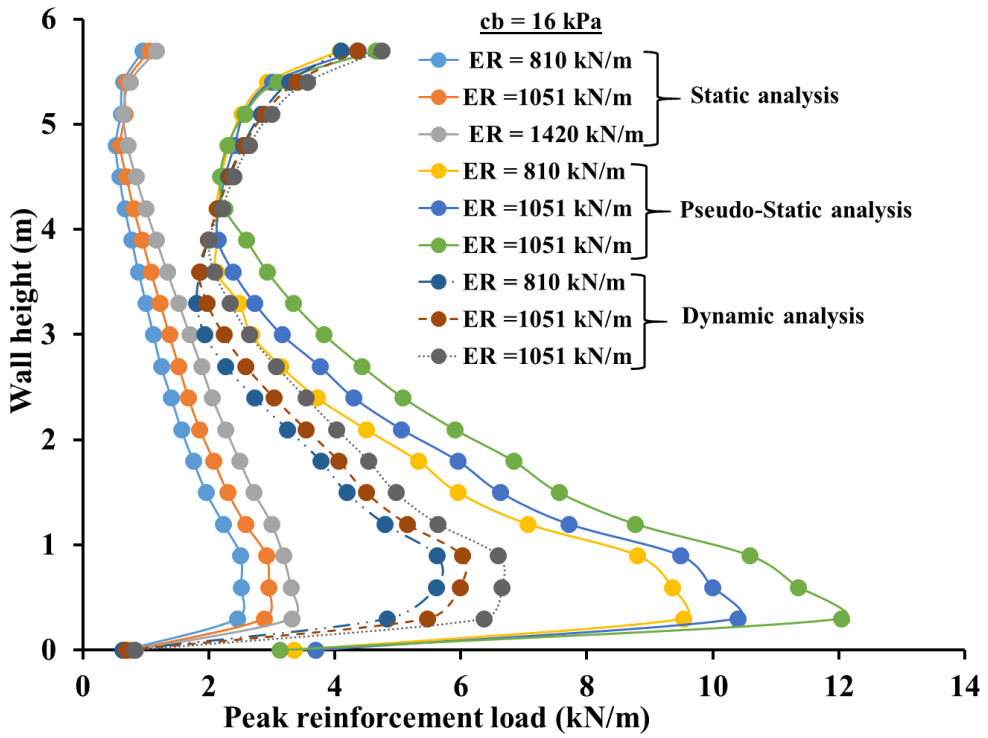

(c)

Fig. 12. Profile of peak reinforcement load in the GRS wall with marginal backfill having cohesion of (a) 5 kPa (b) 10 kPa (c) 16 kPa

Fig. 13(a-c) depicts the time-history of peak mobilized load in the reinforcements of stiffness 1420 kN/m embedded in the marginal backfill of GRS wall having a backfill cohesion of 5 kPa, 10 kPa, and 16 kPa, respectively. It is noted that the maximum reinforcement load was mobilized across all layers within 15 seconds when subjected to the input motion. This is attributed to the fact that the peak ground acceleration (PGA) of the chosen 1995 Kobe strong motion occurs during this time-frame that imposes higher dynamic forces on the GRS wall structure. Fig. 13(d) summarizes that backfill cohesion significantly influences reinforcement load mobilization, indicated by notably varied profiles of peak load along the depth of the wall.

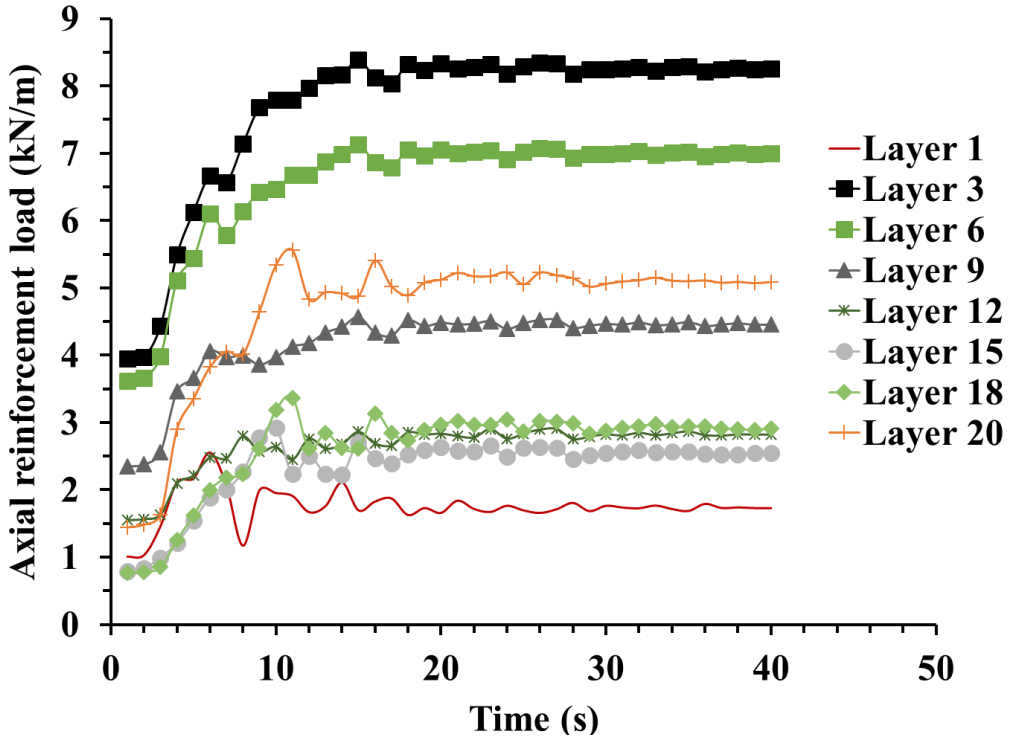
Axial reinforcement load (kN/m)
Time (s)
Layer 1
Layer 3
Layer 6
Layer 9
Layer 12
Layer 15
Layer 18
Layer 20

579 (a)

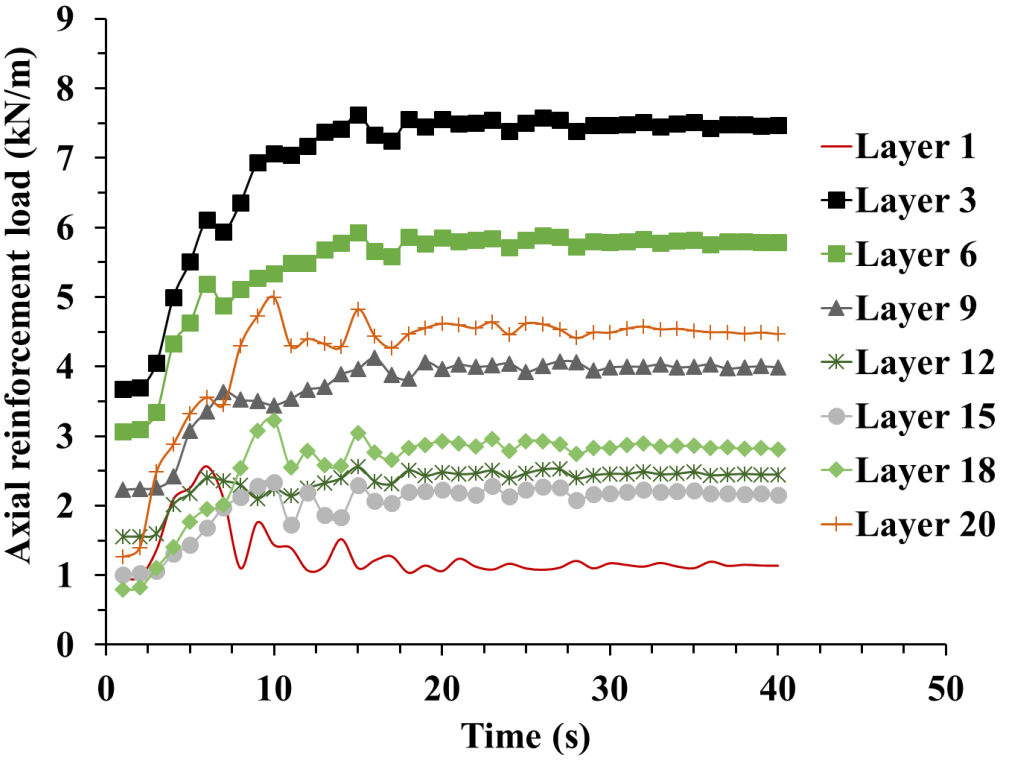
Axial reinforcement load (kN/m)
Time (s)
Layer 1
Layer 3
Layer 6
Layer 9
Layer 12
Layer 15
Layer 18
Layer 20

580 (b)

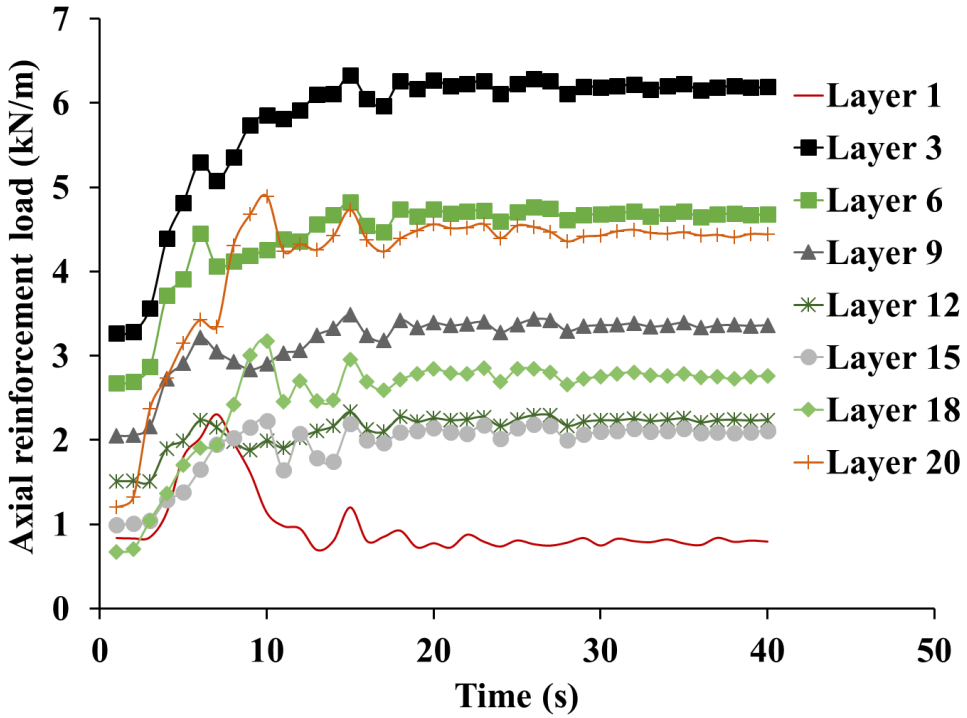

(c)

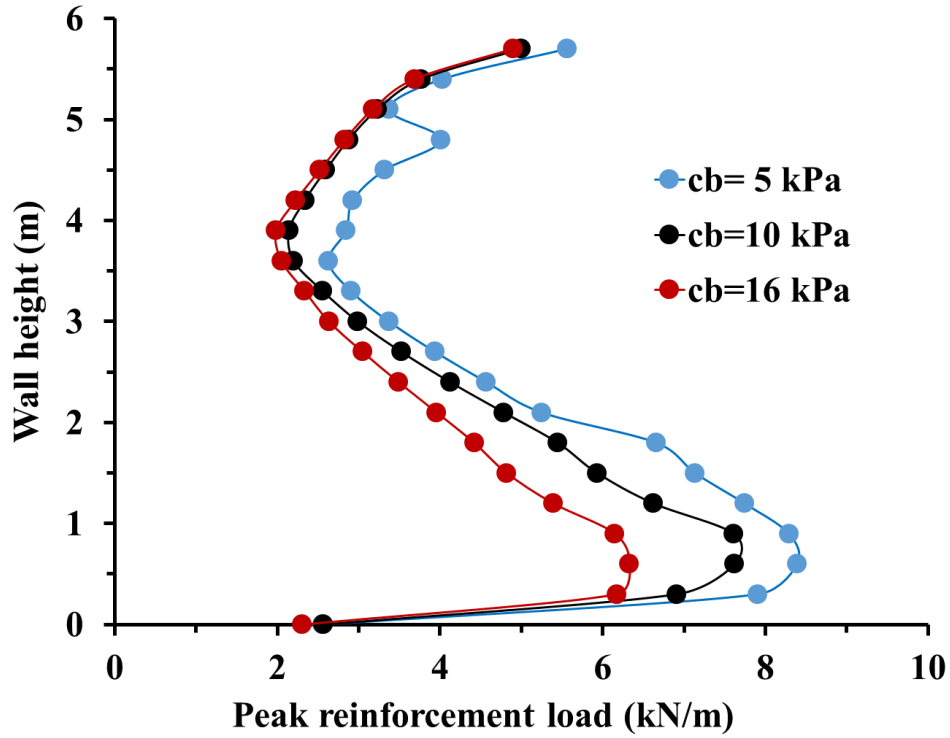

(d)

Fig. 13 Temporal evolution of peak reinforcement load in the GRS wall with marginal backfill having cohesion of (a) 5 kPa (b) 10 kPa (c) 16 kPa, and (d) comparative profile of peak reinforcement load with variation of backfill cohesion of GRS wall with E_R = 1420 kN/m

4.4. Acceleration Amplification Profile of GRS Wall with Marginal Backfill

Krishna and Latha [7] conducted a series of shake table tests on wrap-faced GRS wall concluded that seismic response of GRS wall are affected by base motion parameters, reinforcement configuration and surcharge load. It was found that acceleration amplification towards the crest of a GRS wall is more when a smaller number of reinforcement layer is used in wall system. Kilic *et al*. [25] conducted shake table experiments on GRS walls and observed that the maximum peak amplification values occurred at the top blocks. An amplification factor greater than 3 was found to induce additional stress on the GRS wall, potentially affecting its stability and deformation. Fig. 14 exhibits the representative acceleration time-histories recorded at the GRS wall fascia in few of the reinforcement layers, including the bottommost and topmost ones and corresponding acceleration time-history at points A1, A2, A3 and A4. Based on the acceleration-time histories in all the reinforcements, the amplification factor at various heights is estimated with respect to the acceleration-time history recorded at the bottom of the wall. Fig. 15 illustrates the assessed profiles of acceleration amplification factor (AAF) at the wall face as well as at the end of reinforcement (confined within the marginal backfill), indicating progressively higher amplification towards the top of the wall attributed to the reduction in confinement along the upper stretches of the wall. It can be noted that the AAF along the wall face are higher than that obtained along the end of reinforcement, which is attributed to the fact that the fascia has more flexibility to movement and, hence, contribute to the higher amplifications of earthquake motion propagating from bottom to the top of the GRS wall. It can be noted that the AAF at the upper portions of the GRS wall face exceeds the magnitude of 3, thereby inducing additional stresses in the GRS wall. It can be also comprehended from Fig. 15 that the AAF profiles obtained for GRS wall with backfill cohesions of 10 kPa and 16 kPa are very similar, both qualitatively and quantitatively, with only minor deviations in trends and magnitudes. This behavior is attributed to the fact that once a sufficient cohesion level is reached, the soil gains enough shear strength to resist further significant changes in dynamic response. Additional increases in cohesion have a negligible effect on acceleration amplification as the reinforced soil system already develops adequate resistance against seismic loading. Minor deviations, as noted, may still occur due to local variations in soil-reinforcement interaction and distribution in reinforcement loads and strains.

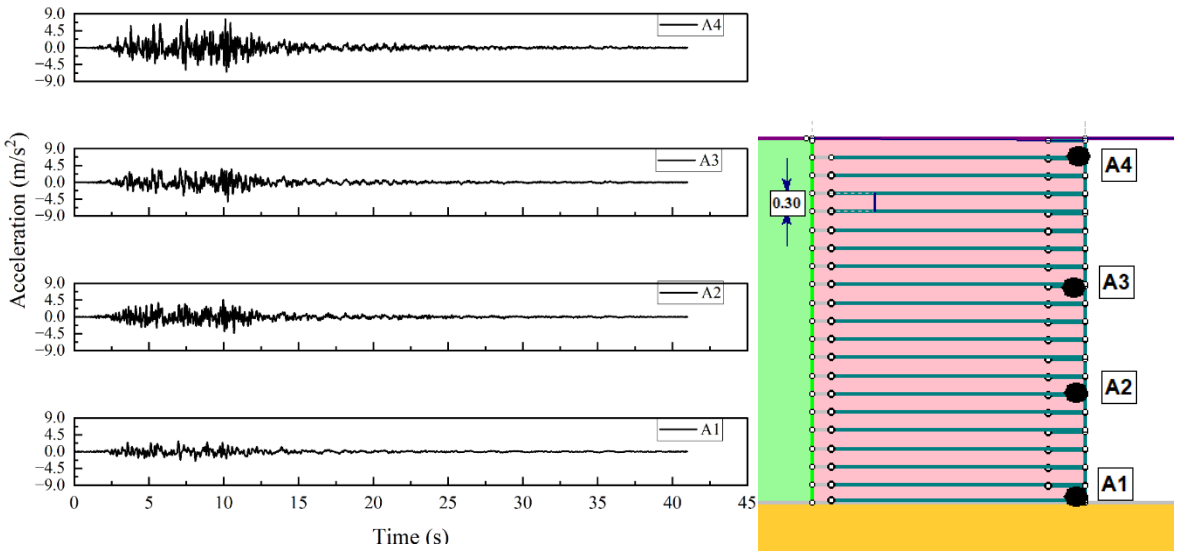

615

616 **Fig. 14.** Acceleration-time history at the wall face for c_b= 16 kPa and E_R= 1420 kN/m

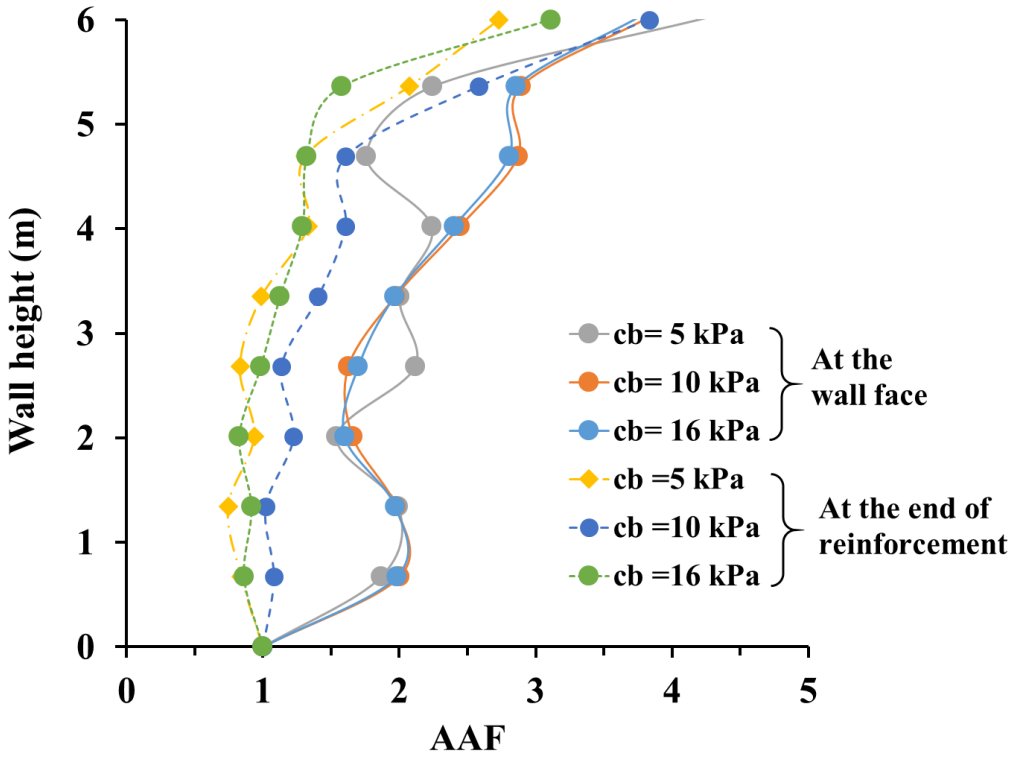

617

618 **Fig. 15.** Profiles of acceleration amplification factor at the wall face and at the end of reinforcement

619 as a function of the cohesion of marginal backfill

620

621

4.5. Peak Reinforcement Strains in GRS Wall with Marginal Backfill

Figures 16, 17, and 18 illustrate the peak strain developed in the geotextile reinforcement at different time instants as the GRA wall with backfill cohesion of 5 kPa, 10 kPa and 16 kPa, respectively, is subjected to 1995 Kobe earthquake motion. The results indicate that an increase in backfill cohesion and reinforcement stiffness reduces the maximum reinforcement strain. Furthermore, the findings show that the maximum reinforcement strain occurs within the first 15 seconds of the Kobe 1995 motion for all reinforcement layers. However, it may be interestingly noted that the strain magnitude is lower in the upper layers, and the peak reinforcement strain occurs in lesser time duration in these layers. This behavior is attributed to the upward propagation of seismic waves, causing the top layers to experience motion and deformation earlier due to their proximity to the free surface. Additionally, higher amplification in the uppermost layers, combined with lower overburden pressure, leads to a greater tendency for reinforcement pullout. In contrast, the strain magnitude is significantly higher in the bottom two-thirds of the wall, where greater confinement and stress accumulation result in higher reinforcement strain. As shown in Figures 16, 17, and 18, the reinforcement strain increases nonlinearly over time until it reaches its peak and then transitions to a residual state. This behavior qualitatively follows the applied earthquake ground motions that typically exhibit a high-intensity shaking at the beginning followed by a gradual reduction in amplitude. As the seismic loading decreases, the reinforcement strain stabilizes to its residual state, thereby indicating a permanent deformation in the reinforcement at the end of the shaking.

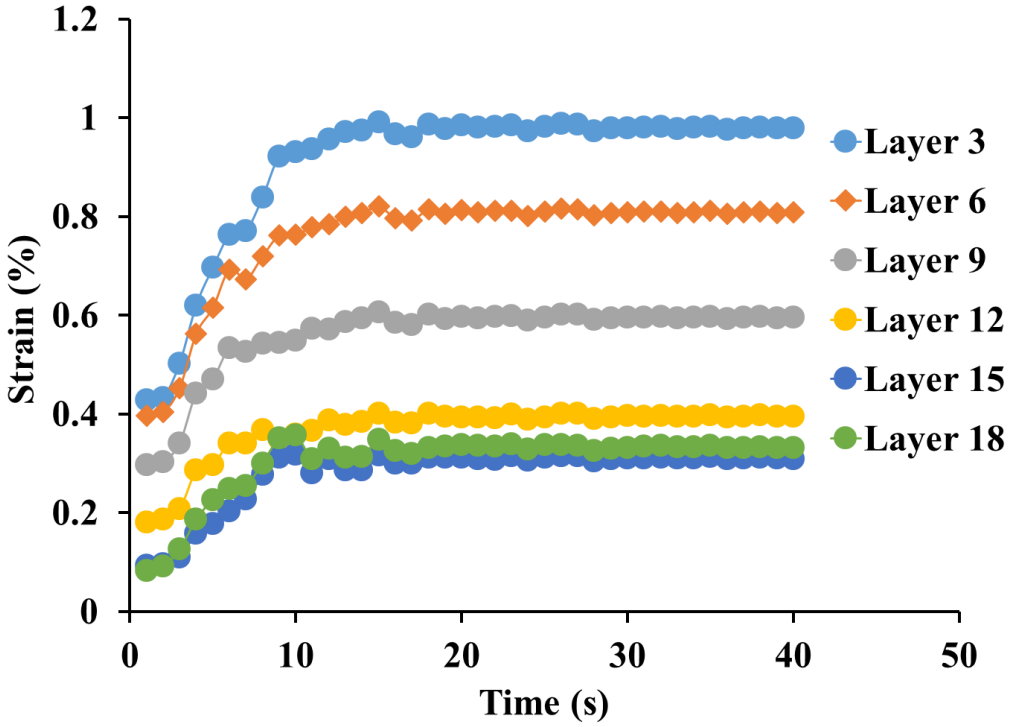
1.2
1
0.8
0.6
0.4
0.2
0
Strain (%)
0
10
20
30
40
50
Time (s)
Layer 3
Layer 6
Layer 9
Layer 12
Layer 15
Layer 18

643 (a)

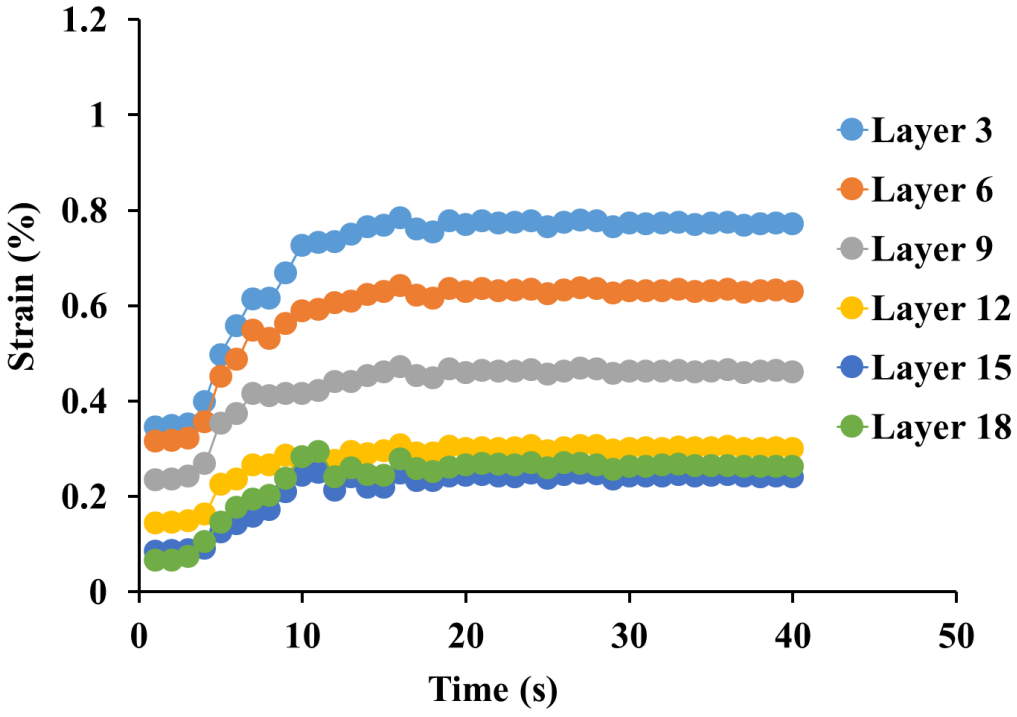
1.2
1
0.8
0.6
0.4
0.2
0
Strain (%)
0
10
20
30
40
50
Time (s)
Layer 3
Layer 6
Layer 9
Layer 12
Layer 15
Layer 18

644 (b)

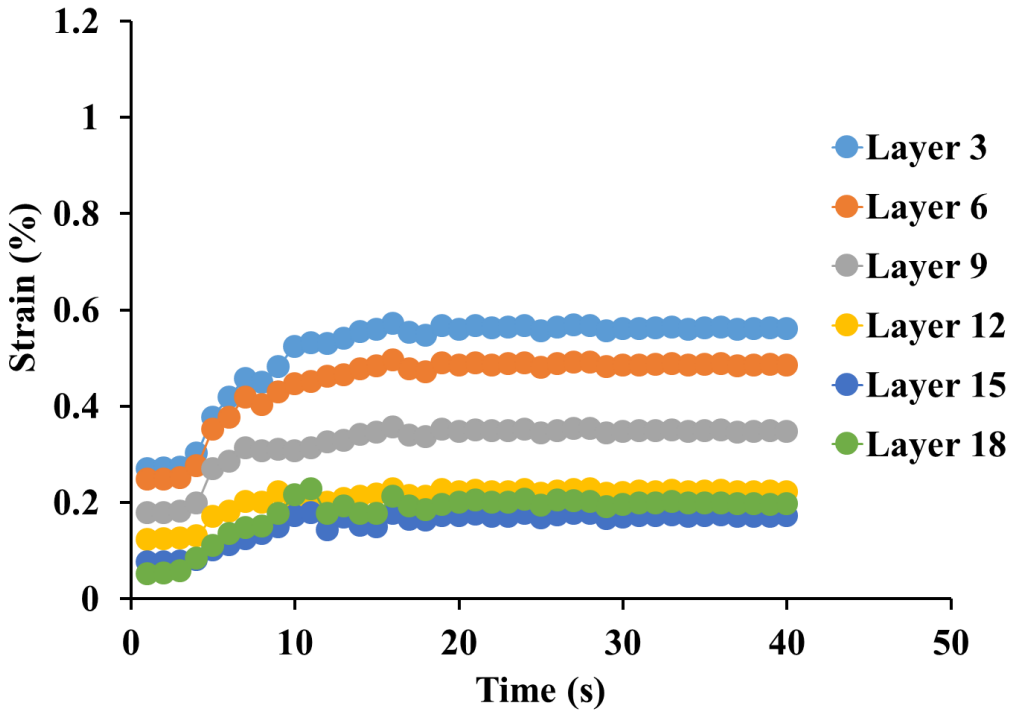

(c)

Fig. 16 Temporal evolution of peak reinforcement strain in the GRS wall with marginal backfill having cohesion of 5 kPa and reinforcement stiffness of (a) 810 kN/m (b) 1051 kN/m (c) 1420 kN/m

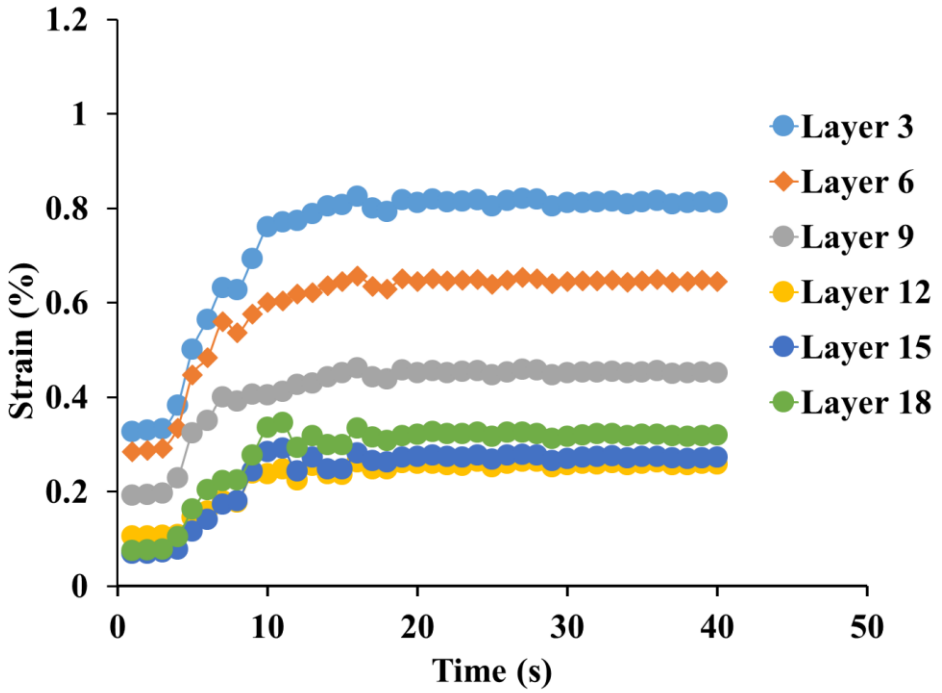
1.2
1
0.8
0.6
0.4
0.2
0
Strain (%)
0
10
20
30
40
50
Time (s)
Layer 3
Layer 6
Layer 9
Layer 12
Layer 15
Layer 18

(a)

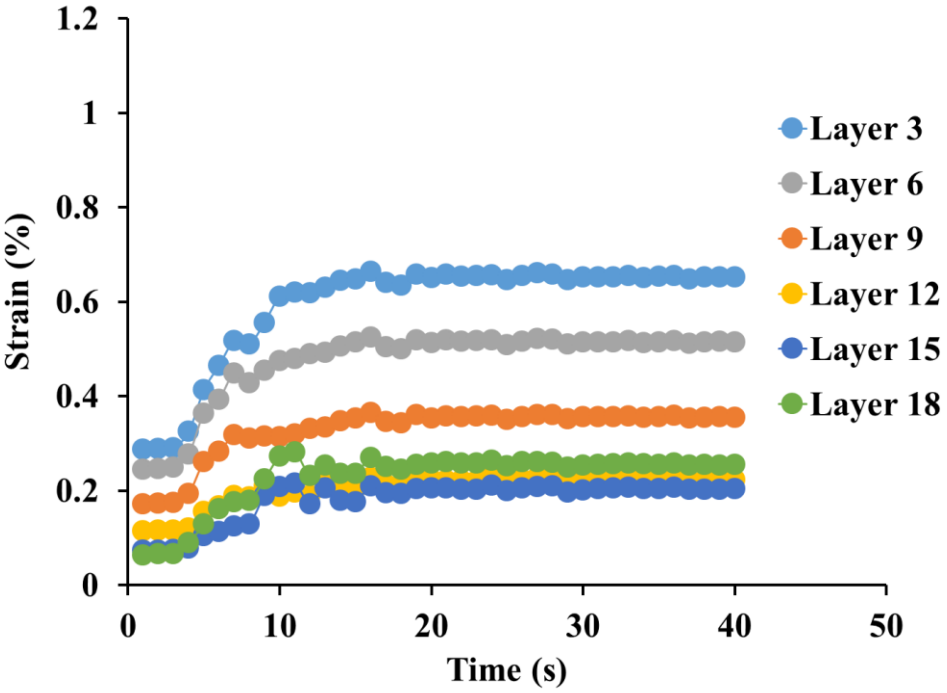
1.2
1
0.8
0.6
0.4
0.2
0
Strain (%)
0
10
20
30
40
50
Time (s)
Layer 3
Layer 6
Layer 9
Layer 12
Layer 15
Layer 18

(b)

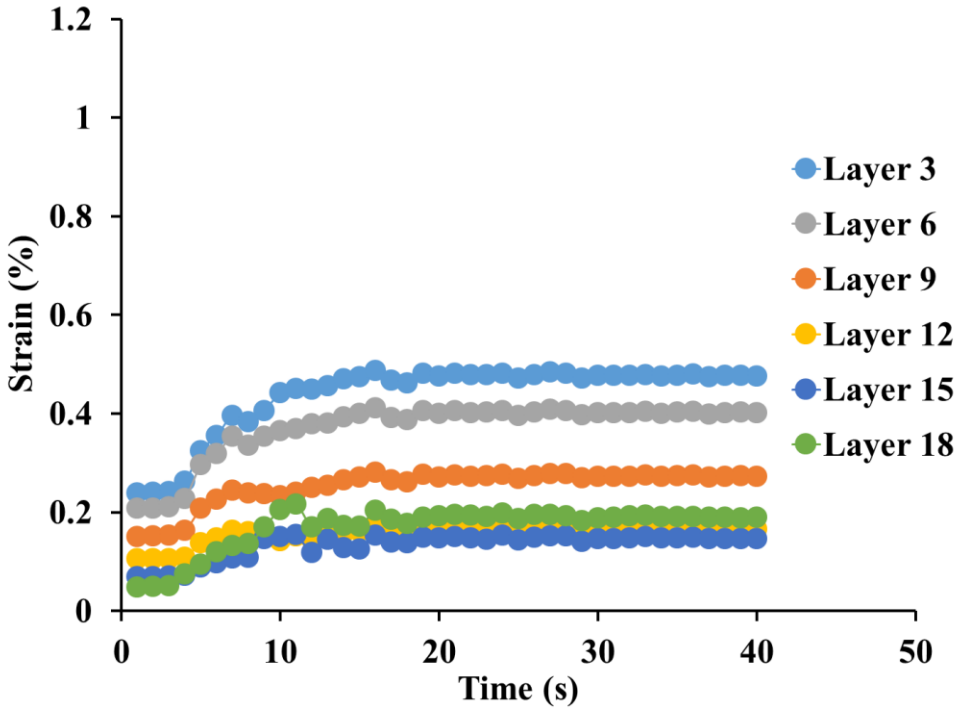

(c)

Fig. 17 Temporal evolution of peak reinforcement strain in the GRS wall with marginal backfill having cohesion of 10 kPa and reinforcement stiffness of (a) 810 kN/m (b) 1051 kN/m (c) 1420 kN/m

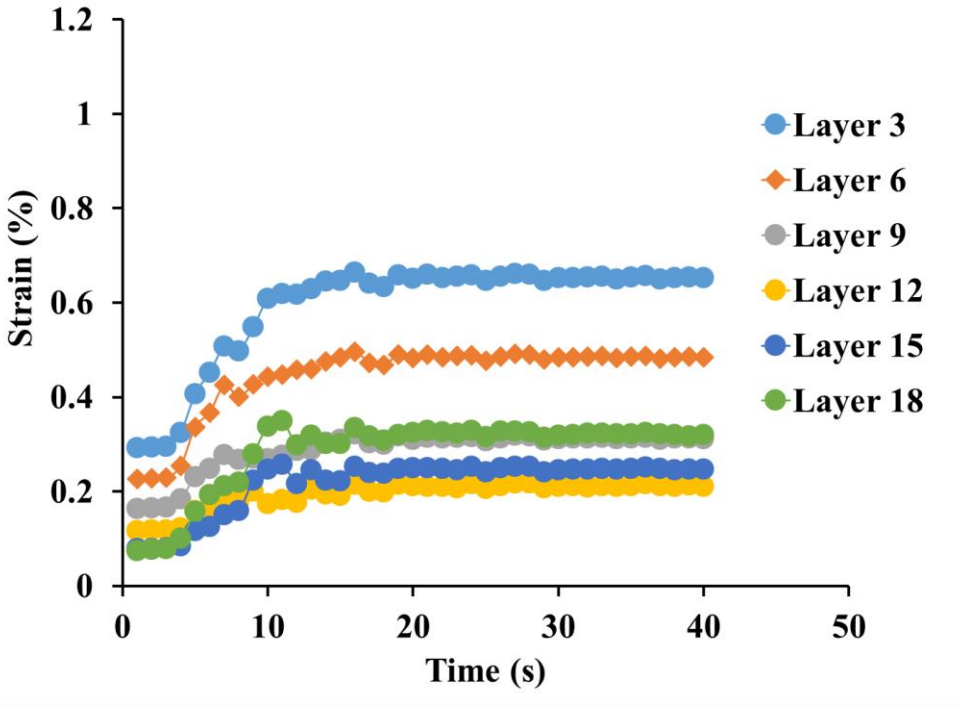

(a)

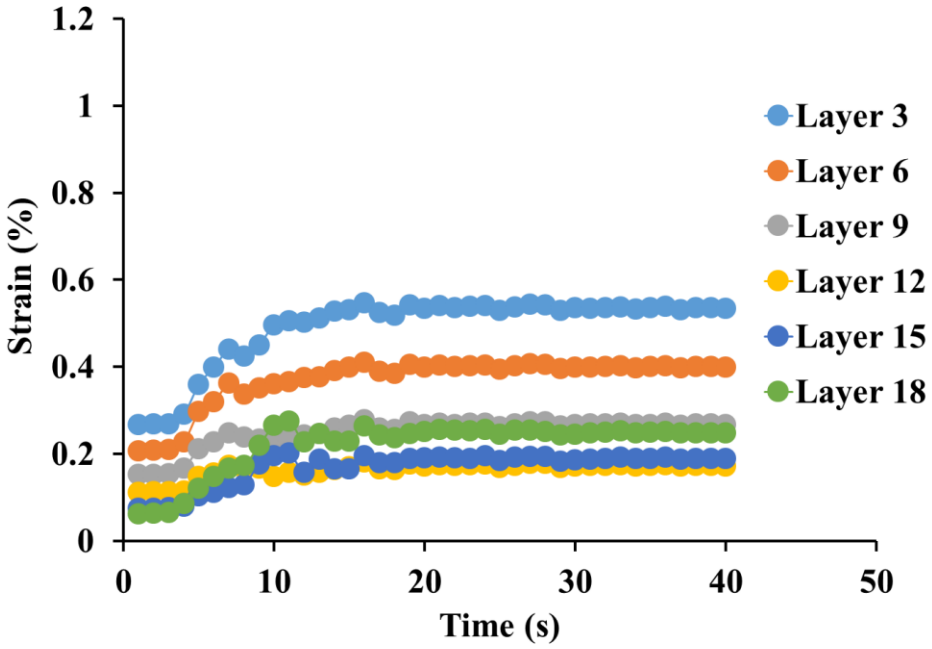

(b)

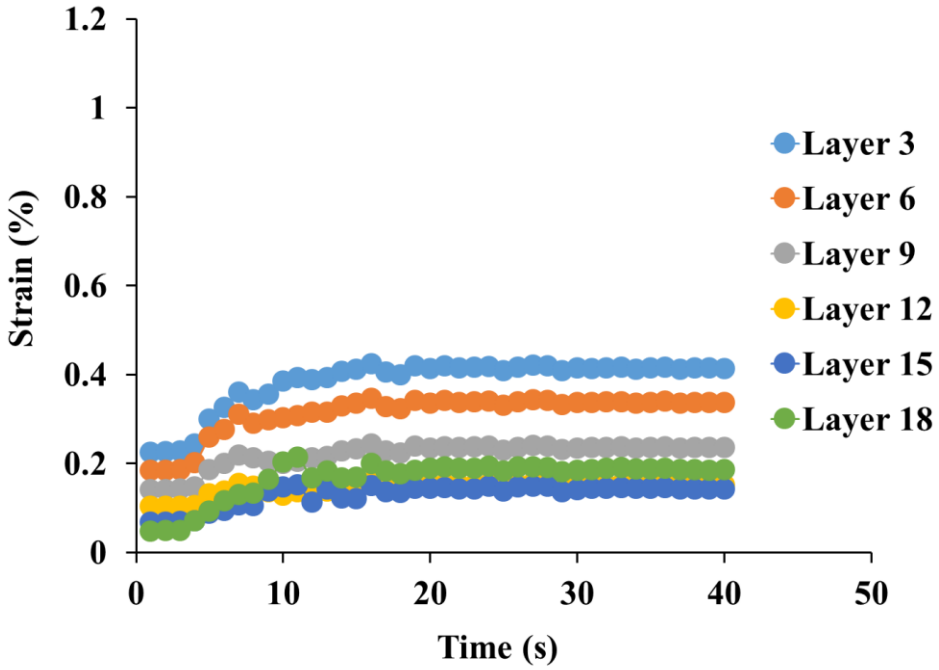

(c)

Fig. 18 Temporal evolution of peak reinforcement strain in the GRS wall with marginal backfill having cohesion of 16 kPa and reinforcement stiffness of (a) 810 kN/m (b) 1051 kN/m (c) 1420 kN/m

4.6. Potential Failure Plane in GRS Wall with Marginal Backfill

The potential failure surface in any retention structure is typically determined from the locations of maximum shear strain or plastic strain developed in the backfill and the reinforcements [44]. In GRS walls, while the reinforced zone is treated as a single block in external stability analysis, internal stability assessment necessitates evaluating the potential failure surface within the reinforced zone. This is critical to identify the reinforcement carrying the maximum axial load and its typology of failure, thereby indexing the reinforcement having the potential to failure. Such evaluations are important for optimizing the tensile strength of reinforcement layers, ensuring efficient material use, and avoiding overdesign, which could lead to unnecessary economic issues. In general, the locus of the peak strains occurring in the reinforcement layers coincide with the peak load developed in the corresponding reinforcement layers [45]. Hence, under dynamic conditions, it is a common practice to identify the potential failure line following the locus of the peak reinforcement load developed in various geosynthetic reinforcement layers [44-46].

The lateral stress at the PGA (i.e. 7^{th} second time instant) of the Kobe 1995 earthquake motion is considered to illustrate the stress concentration pattern within the GRS wall system. As shown in Fig. 19, the concentration of lateral stresses is most prominent in the bottom half of the GRS wall fascia. This is primarily because the lower portion of the wall carries the highest overburden pressure from the retained and reinforced fill above it, in addition to the inertial forces generated during seismic loading. The combined effect of these vertical and horizontal forces leads to higher confinement and greater stress transfer toward the fascia in this zone. As the height increases toward the top half of the wall, the magnitude of overburden pressure decreases. Consequently, the lateral stress concentration diminishes in this region, as less soil mass contributes to seismic inertial loading and confinement is relatively lesser. A second zone of stress concentration is observed near the interface between the reinforced fill and the retained fill. This arises due to the stiffness contrast between the two zones: the reinforced fill, being confined by reinforcement, resists lateral deformation more effectively, while the retained fill undergoes relatively larger displacements. This differential movement generates stress concentration along the interface, reflecting the transfer of seismic-induced forces across the boundary.

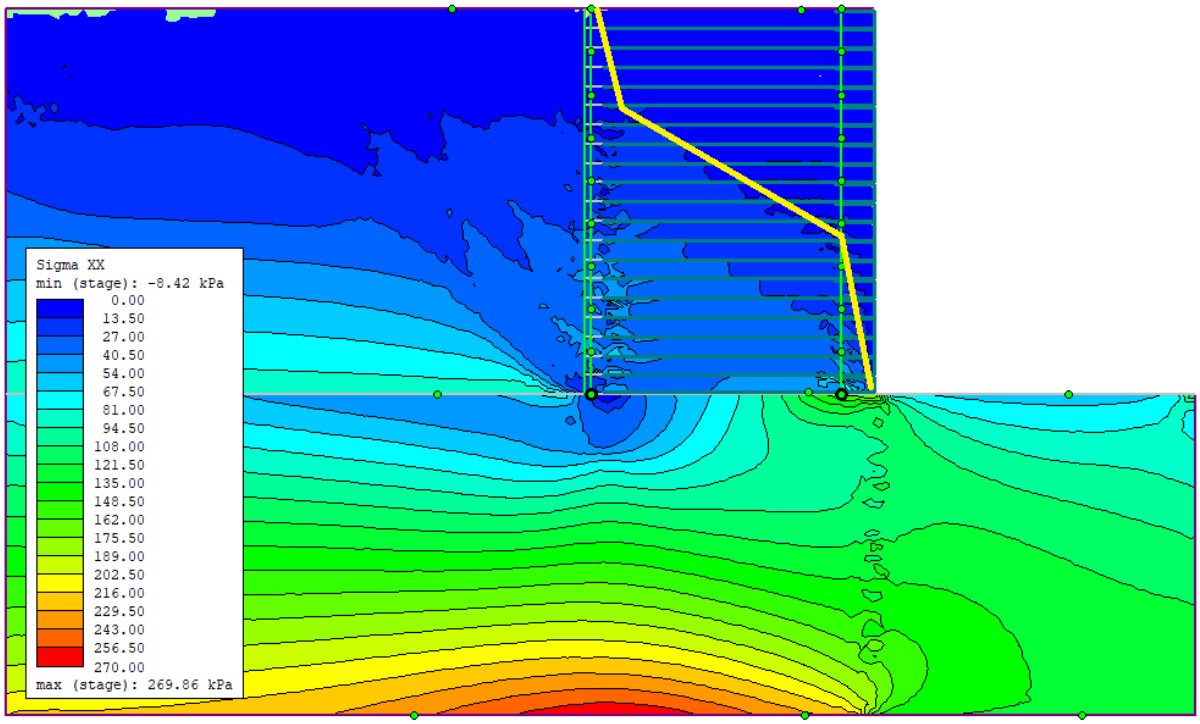

Fig. 19. Lateral stress distribution from dynamic analysis of a GRS wall with c_b = 10 kPa and E_R = 1420 kN/m at PGA (i.e. at 7th second time instant)

Following the established guideline, in the present study, Fig. 20 illustrates the potential failure surfaces recognized by following the locus of the peak reinforcement load trajectories for GRS walls, with various combinations of backfill cohesion and reinforcement stiffness, developed under various types of analyses. It can be noted from Fig. 20 that across all analyses and variations in backfill and reinforcement materials, the bottom one-third of the wall consistently indicates the locus of peak reinforcement load, i.e. the potential failure plane, situated near the wall fascia (0.7 m from wall face). This is primarily due to tensile failure in the reinforcements caused by significant overburden pressure. Additionally, the flexible behavior of the wraparound face allows stress to be released at the wall face, while the restrained portions of the reinforcement relatively away from the face sustain higher stresses.

At the uppermost layers, the potential failure surface again shifts closer to the wall face. This behavior is attributed to the cohesive nature of marginal backfill soils, which tend to generate tensile crack at the top of the wall if reinforcement is not provided. Consequently, the maximum reinforcement load is mobilized nearer the face as representatively shown in Fig. 21 for a GRS

713 wall with varying backfill cohesion and reinforced by geosynthetics of stiffness 1420 kN/m. Fig.
714 21(d) shows that the potential failure surfaces developed in the GRS wall. It may be comprehended
715 that the variation in backfill cohesion does not significantly alter the potential failure surface, while
716 reinforcement stiffness is found to have recognizable influence (as shown in Fig. 20). In the mid-
717 height section of the GRS wall, the potential failure surface is found slightly far from the wall face,
718 which is attributed to the reduction in overburden stress due to the relaxation induced by the
719 outward flexible deformation of the wrap-face.
720
721 It is a common practice to design the GRS walls based on the internal stability analysis conducted
722 with an assumed failure surface passing through the reinforcement, and in most cases, the
723 Rankine's failure surface for the active state is used for the assessment [47]. It may be clearly
724 noted from Fig. 21(d) that the potential failure surface obtained from dynamic analysis is
725 approximate with Rankine's triangular wedge failure theory. Not only for the dynamic analysis, it
726 may be noted from Fig. 20 that the potential failure surface for the pseudo-static analysis is also
727 approximately matching with the commonly assumed Rankine's failure surface even though the
728 location of failure pattern does not follow the exact triangular wedge failure. Even the failure
729 surface developed through the GRS wall does not ideally follow the Rankine's failure surface
730 which is more suitable for the backfill soils without any other composite inclusions. Hence, the
731 conventional practice of conducting internal stability analysis of GRS wall considering a Rankine
732 failure surface based on the frictional characteristics of the backfill [5] needs modification,
733 especially for a wrap-faced GRS wall structure, that too from an analysis perspective.
734
735
736
737
738

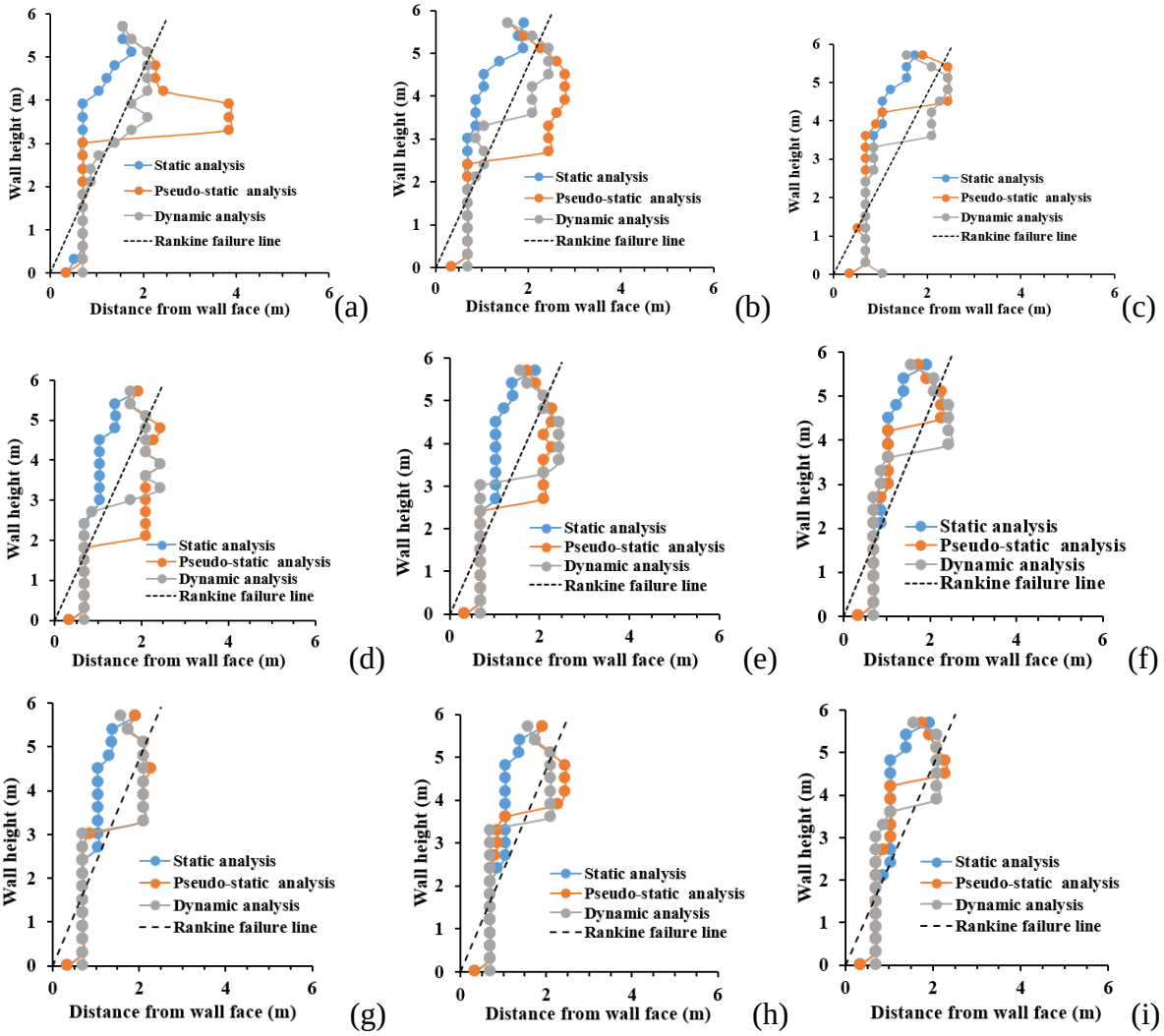

Fig. 20. Potential failure surface of the wrap-faced GRS wall with (a) c_b = 5 kPa, E_R = 810 kN/m (b) c_b = 10 kPa, E_R = 810 kN/m (c) c_b = 16 kPa, E_R = 810 kN/m (d) c_b = 5 kPa, E_R = 1051 kN/m (e) c_b = 10 kPa, E_R = 1051 kN/m (f) c_b = 16 kPa, E_R = 1051 kN/m (g) c_b = 5 kPa, E_R = 1420 kN/m (h) c_b = 10 kPa, E_R = 1420 kN/m (i) c_b = 16 kPa, E_R = 1420 kN/m

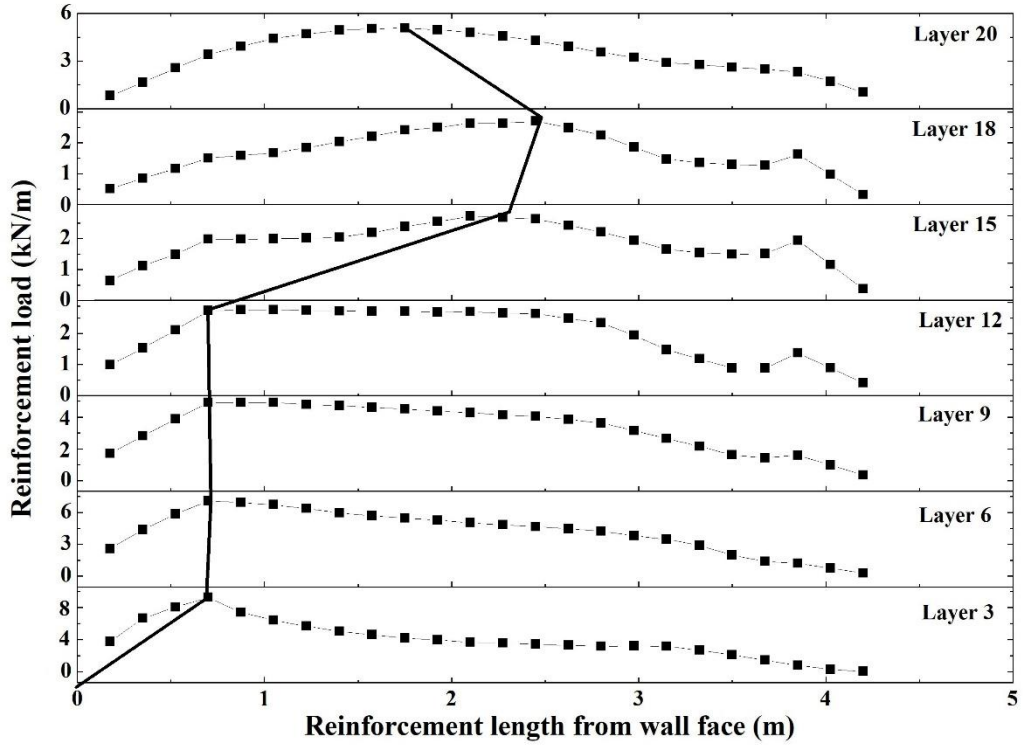
Layer 20
Layer 18
Layer 15
Layer 12
Layer 9
Layer 6
Layer 3
Reinforcement load (kN/m)
Reinforcement length from wall face (m)

747 (a)

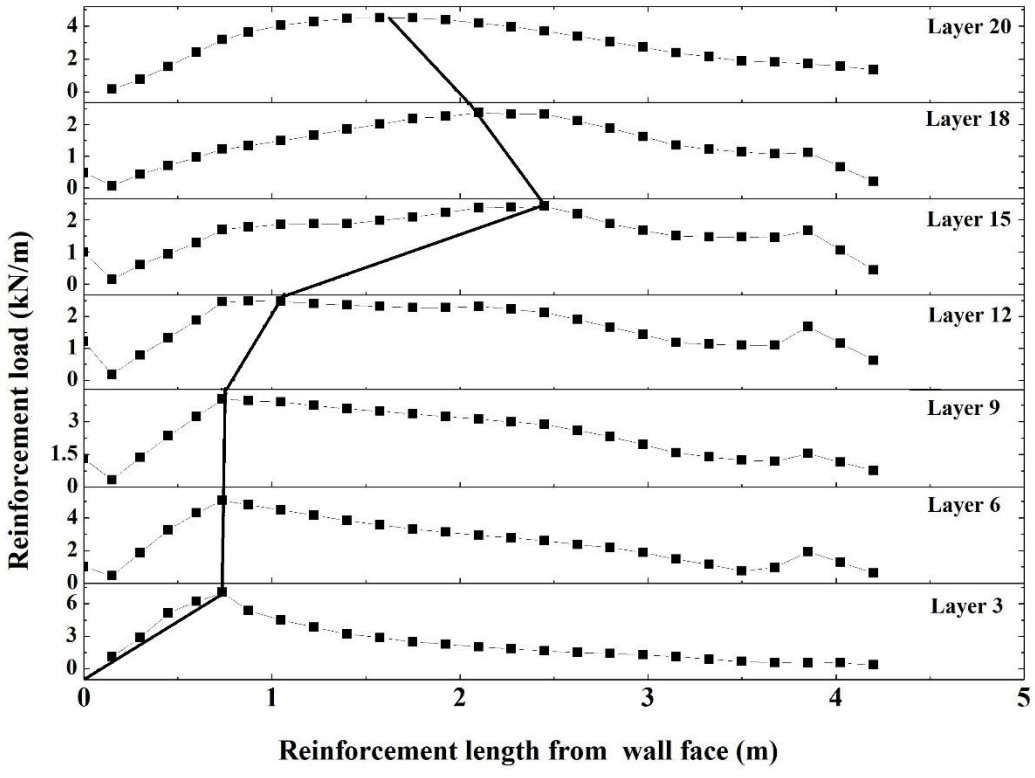
Layer 20
Layer 18
Layer 15
Layer 12
Layer 9
Layer 6
Layer 3
Reinforcement load (kN/m)
Reinforcement length from wall face (m)

748 (b)

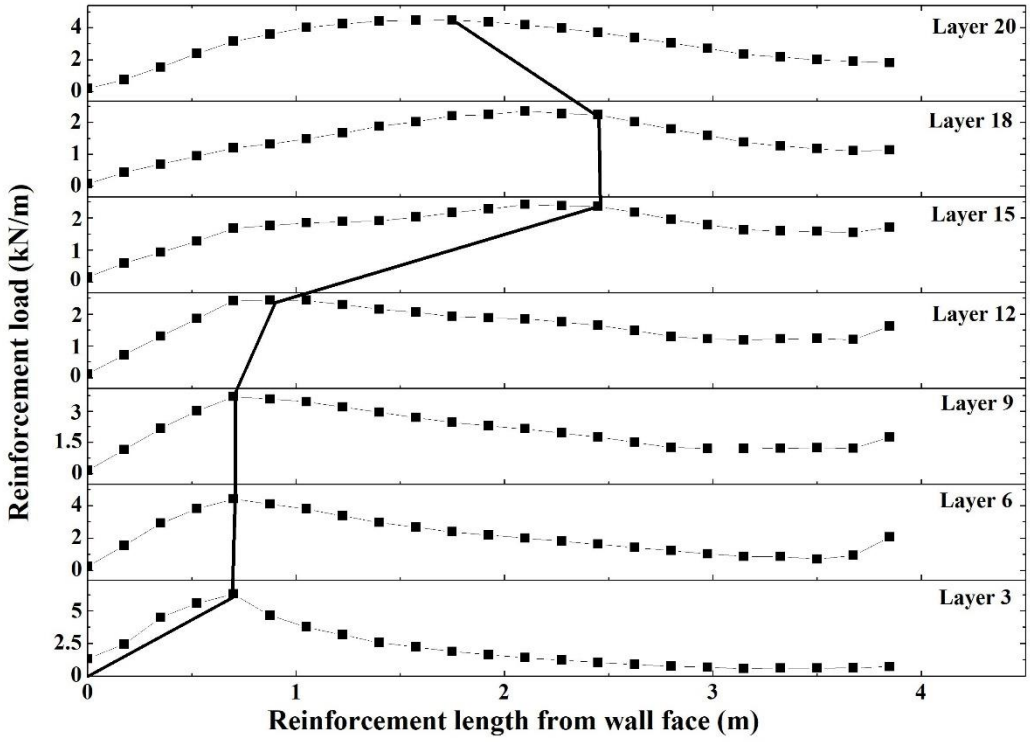

(c)

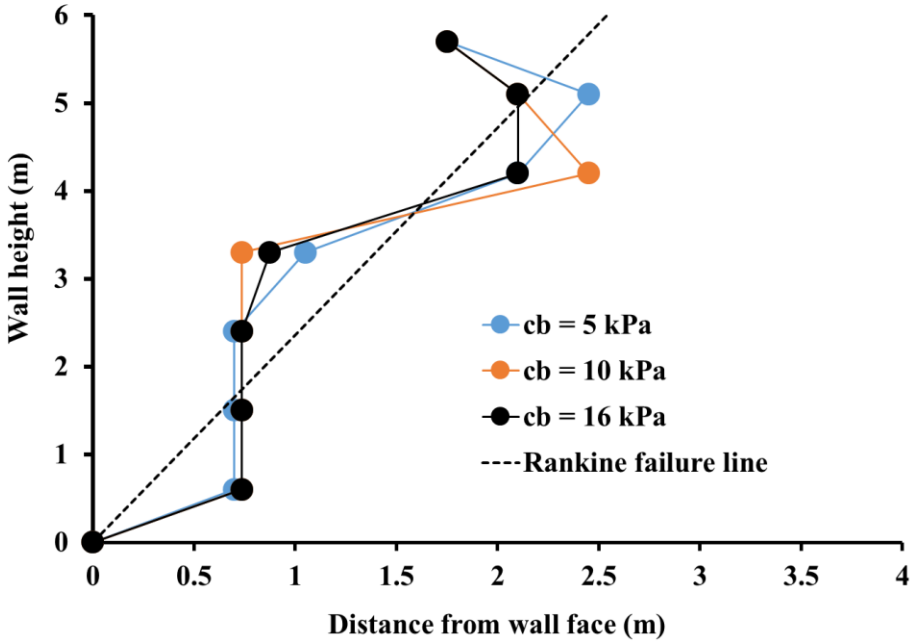

(d)

Fig. 21. Potential failure plane identified as the locus of peak reinforcement load for a dynamic analysis of GRS wall with E_R = 1420 kN/m and backfill cohesion of (a) 5 kPa (b) 10 kPa (c)16 kPa and (d) comparison with conventionally assumed Rankine's failure plane

6 CONCLUSIONS

This study conducted two-dimensional numerical simulations to analyze the effects of parametric variations in reinforced zone backfill soil cohesion and reinforcement stiffness. The seismic analysis of wraparound-face GRS walls with marginal backfill soils focused on key factors influencing wall stability, wall face deformation, reinforcement force, acceleration amplification along wall height and reinforcement strain under static, pseudo-static, and dynamic conditions. The findings show the critical role of reinforcement stiffness and backfill cohesion in seismic performance. Based on the present study, the following conclusions can be drawn:

- Due to the outward movement of the wrap-faced GRS wall, under gravity loading condition, the retained fill exhibits a triangular failure wedge whose inclination is substantially flatter (45° from the present study in comparison to 60° from Rankine's theory), owing to the alteration of the natural failure mechanism and the constraint provided by the GRS wall itself. On the other hand, the reinforced fill exhibit a potential bilinear failure mechanism due to the stabilizing effect from the embedded geotextile reinforcements.
- Reinforcements of higher stiffness leads to distribution of shear stress in the reinforced fill, thereby restraining the displacement in the GRS wall. At the critical stability stage during pseudo-static loading, the presence of wrap-faced GRS wall confines the maximum shear strain bands deep within the retained fill.
- Compared to static analyses, the dynamic time-history analyses approximately exhibits an approximately 1.5 times higher SRF (computed just beyond the time to PGA). This is phenomenological system stability is attributed to stress reversals, cyclic interlocking, energy dissipation, and redistribution of stresses within the reinforced marginal backfill. In comparison to the reinforcement stiffness, cohesion of the marginal backfill is found to be more influential in enhancing the stability under dynamic conditions.
- Under pseudo-static conditions with PGA-based time-independent acceleration coefficients, even if the wrap-faced GRS wall exhibit a substantial stress-based failure marked by SRF < 1, yet the dynamic time-history analysis can exhibit sufficiently high SRF owing to the cyclic stress reversals, stress redistribution within the reinforced fill and momentary occurrence of PGA. This understanding further renders the conservativeness

of pseudo-static analysis in design practices, often leading to cumbersome and uneconomical designs.

- Under static conditions, wall-face displacement is minimally affected by backfill cohesion or reinforcement stiffness, with a maximum variation of only 5 mm, reflecting the limited influence of marginal backfill strength parameter on lateral deformation. Due to additional inertial forces, pseudo-static assessment expectedly shows higher lateral displacement of the wall. The displacement magnitude is found to be prominently influenced by the change in reinforcement stiffness, although the effect gets diminished at higher magnitudes of marginal backfill cohesion.
- Due to internal damping of the flexible wrap-faced GRS wall system, the maximum lateral displacements of the fascia gets reduced by at least 30%-50% of that observed in comparison to the corresponding pseudo-static analysis. This finding highlights the conservativeness of the pseudo-static assessments towards the response of flexible wrap-faced GRS wall.
- Although an increase in the mobilized peak reinforcement load is noted with the increase in reinforcement stiffness under pseudo-static loading, yet the variability is only marginal in case of dynamic assessment. Rather, under dynamic conditions, a three times increment in the marginal backfill cohesion is found to effectively reduce the mobilization of peak reinforcement load by approximately 1.4 times through energy dissipation and reduced friction mobilized at the soil-geosythentic interface.
- A noticeable amplification of peak acceleration, in the range of 2.5-4, is noted from the bottom to the crest of the wrap-faced GRS walls. The AAF achieves higher values along the wall face, nearly 1.5-2 times of that at the reinforcement ends, which is primarily attributed to the reduced confinement and greater fascia flexibility. The influence of the backfill cohesion on the variability of AAF is more prominent over the ones at the reinforcement ends.
- Increment in the cohesion of the marginal backfill and the reinforcement stiffness reduces the peak reinforcement strain. For any parametric state considered, the peak strains in any of the reinforcement layer consistently mobilized within the first 15 seconds of the Kobe 1995 motion, i.e. soon after the time to PGA of the input motion.

- Higher amplification and lower overburden in the upper layers lead to earlier and lower peak strain, whereas the bottom two-thirds of the wall experience greater confinement and stress accumulation, resulting in higher strain that follows a nonlinear time history before stabilizing to a residual state.
- Potential failure surfaces are identified as the locus of the maximum shear strains or peak reinforcement load developed in the reinforcements. It is found to consistently develop at the bottom one-third of the wall, situated near the wall face (approximately 0.7 m from the face) across all analysis types, primarily due to achieving the tensile capacity of the reinforcement under combined overburden and seismic loading. For the upper one-third of the wall height, the potential failure surface takes different loci, depending on the type of analyses, backfill cohesion and the reinforcement stiffness.
- The potential failure surfaces identified under pseudo-static and dynamic time-history analyses exhibit an average agreement to the alignment of Rankine's active failure line, thereby indicating that the latter can be considered for a preliminary design and analysis. However, the stark differences between the potential failure surfaces identified for the GRS walls under static, pseudo-static and dynamic analyses calls for greater scrutiny on the response of such walls so that their potential failure and their corresponding vulnerable hotspots can be prudently captured. Such a step would aid proper and detailed design, rectification or restoration measures to be adopted for wrap-faced GRS walls with marginal backfill.

Author Contribution(s)

MM was involved in conceptualization, methodology, formal analysis, data curation and interpretation, software, validation, visualization, writing-original draft, reviewing and editing. AD was involved in conceptualization, methodology, interpretation, supervision, writing-reviewing and editing.

Funding Statement

This research did not receive any specific grant from funding agencies like public, commercial or non-profit sectors.

Data Availability Statement

Data sets generated during the current study are available from the corresponding author on reasonable request.

Conflict of Interest

The authors declare that they have no conflict of interest.

REFERENCES

1. Tatsuoka F, Koseki J, Kuwano J (2014) Natural disasters mitigation by using construction methods with geosynthetics (earthquakes). In: Proceedings of the 10th International Conference on Geosynthetics, London, 1-53.
2. Wu JT, Ooi PS (2015) Synthesis of geosynthetic reinforced soil (GRS) design topics. Technical Report No. FHWA-HRT-14-094, Department of Civil and Environmental Engineering, University of Hawaii at Manoa for FHWA Research, Development and Technology.
3. Lee KZ, Wu JT (2004) A synthesis of case histories on GRS bridge-supporting structures with flexible facing. Geotextile and Geomembranes, 22(4): 181–204. https://doi.org/10.1016/j.geotexmem.2004.03.002
4. Koerner RM (2005) Designing with Geosynthetics. Pearson Prentice Hall, NJ, USA.
5. Koseki J, Bathurst RJ, Guler E, Kuwano J, Maugeri M (2006) Seismic stability of reinforced soil walls. In: Proceedings of the 8th International Conference on Geosynthetics, 1: 51-78.
6. Ramakrishnan S, Budhu M, Britto A (1998) Laboratory seismic tests of geotextile wrap-faced and geotextile-reinforced segmental retaining walls. Geosynthetics International, 5(1–2): 55–71. https://doi.org/10.1680/gein.5.0114
7. Murali Krishna A, Madhavi Latha G (2007) Seismic response of wrap-faced reinforced soil-retaining wall models using shaking table tests. Geosynthetics International, 14(6): 355–364. https://doi.org/10.1680/gein.2007.14.6.355
8. Huang CC (2019) Seismic responses of vertical-faced wrap-around reinforced soil walls. Geosynthetics International, 26(2): 146–163. https://doi.org/10.1680/jgein.18.00044

9. Hore R, Chakraborty S, Shuvon AM, Ansary MA (2020) Effect of acceleration on wrap faced reinforced soil retaining wall on soft clay by performing shaking table test. Proceedings of Engineering and Technology Innovation, 15: 24-34. https://doi.org/10.46604/peti.2020.4485
10. Chehade HA, Dias D, Sadek M, Jenck O, Chehade FH (2019) Seismic analysis of geosynthetic-reinforced retaining wall in cohesive soils. Geotextiles and Geomembranes, 47(3), 315–326. https://doi.org/10.1016/j.geotexmem.2019.02.003
11. Chehade HA, Dias D, Sadek M, Jenck O, Hage Chehade F (2021) Pseudo-static analysis of reinforced earth retaining walls. Acta Geotechnica, 16: 2275–2289. https://doi.org/10.1016/S0266-352X(98)00016-0
12. Anubhav S, Basudhar PK (2011) Numerical modelling of surface strip footings resting on double-faced wrap-around vertical reinforced soil walls. Geosynthetics International 18(1), 21–34. https://doi.org/10.1680/gein.2011.18.1.21
13. Khosrojerdi M, Xiao M, Qiu T, Nicks J (2017) Evaluation of prediction methods for lateral deformation of GRS walls and abutments. Journal of Geotechnical and Geoenvironmental Engineering ASCE, 143(2), 06016022. https://doi.org/10.1061/(ASCE)GT.1943-5606.0001591
14. Rahmaninezhad SM, Han J (2021) Lateral facing deflections of geosynthetic-reinforced retaining walls under footing loading. Transportation Geotechnics, 30, 100594. https://doi.org/10.1016/j.trgeo.2021.100594
15. Sharma S, Prashant A (2023) Seismic coefficients for pseudo-static analysis of wrap-faced GRS walls with nonlinear soil fills. Soil Dynamics and Earthquake Engineering, 171, 107960. https://doi.org/10.1016/j.soildyn.2023.107960
16. Yu Y, Bathurst RJ, Allen TM (2017) Numerical modelling of two full-scale reinforced soil wrapped-face walls. Geotextiles and Geomembranes, 45(4), 237–249. https://doi.org/10.1016/j.geotexmem.2017.02.004
17. Berg RR, Samtani NC, Christopher BR (2009) Design of mechanically stabilized earth walls and reinforced soil slopes–Volume II. FHWA-NHI-10-025, U.S. Department of Transportation, Federal Highway Administration. https://rosap.ntl.bts.gov/view/dot/49730
18. BS 8006-1 (2010) Code of practice for strengthened/reinforced soils and other fills. British Standards Institute.

19. IRC SP102 (2014) Guidelines for design and construction of reinforced soil walls. Indian Roads Congress, New Delhi.
20. NCMA (2010). Design manual for segmental retaining walls. 3rd Edition, National Concrete Masonry Association.
21. Ragon PL, Rodríguez F (2021) CO_2 emissions from trucks in the EU: An analysis of the heavy-duty CO_2 standards baseline data. Working paper, International Council on Clean Transportation, 1-27. https://shorturl.at/jWnJ3
22. Deger TT, Guler E (2024) A case study of a 42-m high GRS retaining structure and CO_2 footprint reduction due to the use of marginal backfill available on site. International Journal of Geosynthetics and Ground Engineering, 10(3), 37. https://doi.org/10.1007/s40891-024-00553-3
23. Liu H, Wang X, Song E (2009) Long-term behavior of GRS retaining walls with marginal backfill soils. Geotextiles and Geomembranes. 27(4), 295-307. https://doi.org/10.1016/j.geotexmem.2009.01.002
24. Balakrishnan S, Viswanadham BVS (2016) Performance evaluation of geogrid reinforced soil walls with marginal backfills through centrifuge model tests. Geotextiles Geomembranes. 44(1), 95-108. https://doi.org/10.1016/j.geotexmem.2015.06.002
25. Kilic IE, Cengiz C, Edincliler A, Guler E (2021) Seismic behavior of geosynthetic-reinforced retaining walls backfilled with cohesive soil. Geotextiles and Geomembranes. 49(5), 1256-1269. https://doi.org/10.1016/j.geotexmem.2021.04.004
26. Li ZW, Yang XL (2020) Seismic analysis of 3D geosynthetic-reinforced soil structures in cohesive backfills with cracks. Geotextiles and Geomembranes. 48(5), 691-702. https://doi.org/10.1016/j.geotexmem.2020.04.003
27. Samtani NC, Nowatzki EA (2021) Mechanically stabilized earth (MSE) wall fills: A framework for use of local available sustainable resources (LASR). Report No. FHWA-HIN-21-002, FHWA US Department of Transportation, Federal Highway Administration, Central Federal Lands Highway Division, Colorado, USA.
28. Majumder M, Venkatraman S, Bheda M, Patil M (2023) Numerical studies on the performance of geosynthetic reinforced soil walls filled with marginal soil. Indian Geotechnical Journal, 53(4), 805-826. https://doi.org/10.1007/s40098-022-00706-z

29. Abu-Farsakh MY, Almohd I, Farrag K (2006) Comparison of field and laboratory pullout tests on geosynthetics in marginal soils. Transportation Research Record, 1975(1), 124-136. https://doi.org/10.1177/0361198106197500114
30. Abdi MR, Arjomand MA (2011) Pullout tests conducted on clay reinforced with geogrid encapsulated in thin layers of sand. Geotextiles and Geomembranes, 29(6), 588-595. https://doi.org/10.1016/j.geotexmem.2011.04.004
31. Pierozan RC, Araujo GLS, Palmeira EM, Romanel C, Zornberg JG (2022) Interface pullout resistance of polymeric strips embedded in marginal tropical soils. Geotextiles and Geomembranes, 50(1), 20-39. https://doi.org/10.1016/j.geotexmem.2021.08.004
32. Yu Y, Bathurst RJ, Allen TM, Nelson R (2016) Physical and numerical modelling of a geogrid-reinforced incremental concrete panel retaining wall. Canadian Geotechnical Journal, 53(12), 1883-1901. https://doi.org/10.1139/cgj-2016-0207
33. Potgieter JT, Jacobsz SW (2019) Comparing the factors of safety from finite element and limit equilibrium analyses in lateral support design. Journal of the South African Institution of Civil Engineering, 61(4), 29-41. https://doi.org/10.17159/2309-8775/2019/v61n4a3
34. Mihretab M, Sarma NJ, Sureka S, Dey A (2025) Seismic response of a wrap-face geosynthetic reinforced soil (GRS) wall located on a hillslope in north-east India. Lecture Notes in Civil Engineering Vol. 568: Analyses for Retaining Walls, Slope Stability and Landslides: Select Proceedings of 8th ICRAGEE 2024, Ed(s). R. Sarkar, B. K. Maheshwari and A. Kumar, Springer Nature, Singapore, pp. 49-60, ISBN No. 978-981-96-1682-4. https://doi.org/10.1007/978-981-96-1683-1_5
35. Dawson EM, Roth WH, Drescher A (1999) Slope stability analysis by strength reduction. Geotechnique, 49(6), 835-840. https://doi.org/10.1680/geot.1999.49.6.835
36. Mazindrani ZH, Ganjali MH (1997) Lateral earth pressure problem of cohesive backfill with inclined surface. Journal of Geotechnical and Geoenvironmental Engineering ASCE, 123(2), 11-112. https://doi.org/10.1061/(ASCE)1090-0241(1997)123:2(110)
37. Qin C, Chian SC (2020) Pseudo-dynamic lateral earth pressures on rigid walls with varying cohesive-frictional backfill. Computers and Geotechnics, 119, 103289. https://doi.org/10.1016/j.compgeo.2019.103289

964 38. Luo F, Zhang G, Yao Y (2025) Macro-micro tests of cohesive soil under varied normal and
965 shear stresses subjected to drying-wetting cycles. Journal of Rock Mechanics and
966 Geotechnical Engineering, 17, 5893-5905. https://doi.org/10.1016/j.jrmge.2024.11.007
967 39. Basha BM, Babu GS (2009) Earthquake resistant design of reinforced soil structures using
968 pseudo static method. American Journal of Engineering and Applied Sciences, 2(3), 565-
969 572. https://doi.org/10.3844/ajeassp.2009.565.572
970 40. Pandya S, Sachan A (2022) Effect of frequency and amplitude on dynamic behaviour,
971 stiffness degradation and energy dissipation of saturated cohesive soil. Geomechanics and
972 Geoenginering, 17(1), 30-44. https://doi.org/10.1080/17486025.2019.1680885
973 41. Yang KH, Yalew WM, Nguyen MD (2016) Behavior of geotextile-reinforced clay with a
974 coarse material sandwich technique under unconsolidated-undrained triaxial compression.
975 International Journal of Geomechanics ASCE, 16(3), 04015083.
976 https://doi.org/10.1061/(ASCE)GM.1943-5622.0000611
977 42. Razeghi HR, Ensani A (2023) Clayey sand soil interactions with geogrids and geotextiles
978 using large-scale direct shear tests. International Journal of Geosynthetics and Ground
979 Engineering, 9(2), 24. https://doi.org/10.1007/s40891-023-00443-0
980 43. Liu H, Wang X, Song E (2011) Reinforcement load and deformation mode of geosynthetic-
981 reinforced soil walls subject to seismic loading during service life. Geotextiles and
982 Geomembranes, 29(1), 1-16. https://doi.org/10.1016/
983 j.geotexmem.2010.06.003
984 44. Yang KH, Wu HM, Tseng TL, Yoo C (2023) Model tests of geosynthetic-reinforced soil
985 walls with marginal backfill subjected to rainfall. Geotextiles and Geomembranes, 51(2),
986 342-359. https://doi.org/10.1016/j.geotexmem.2022.12.002
987 45. Zornberg JG, Arriaga F (2003) Strain distribution within geosynthetic-reinforced slopes.
988 Journal of Geotechnical and Geoenvironmental Engineering ASCE, 129(1), 32-45.
989 https://doi.org/10.1061/(ASCE)1090-0241(2003)129:1(32)
990 46. Zornberg JG, Sitar N, Mitchell JK (1998) Performance of geosynthetic reinforced slopes at
991 failure. Journal of Geotechnical and Geoenvironmental Engineering ASCE, 124(8), 670-
992 683. https://doi.org/10.1061/(ASCE)1090-0241(1998)124:8(670)

47. Yang KH, Zornberg JG, Liu CN, Lin HD (2012) Stress distribution and development within geosynthetic-reinforced soil slopes. Geosynthetics International, 19(1), 62-78. https://doi.org/10.1680/gein.2012.19.1.62